Genome-wide insights into the shared genetic landscape between metabolic dysfunction-associated fatty liver disease and cardiovascular diseases

Jun Qiao[1,2,9], Miaoran Chen[3,9], Minjing Chang[4,9], Wenjia Xie[3], Wenqi Ma[3], Tongtong Yang[3], Qianru Zhao[3], Kaixin Yao[3], Xichen Yang[3], Quan Yun[3], Jing Xiao[2,5], Xu He[2,5], Wen Su[6*], Tao Xu[7,8*], Yuliang Feng[1,10*], Meixiao Zhan[2,5*]

[1] Department of Pharmacology, Joint Laboratory of Guangdong-Hong Kong Universities for Vascular Homeostasis and Diseases, School of Medicine, Southern University of Science and Technology, Shenzhen, China.

[2] Guangzhou First Pepople's Hospital, the Second Affiliated Hospital, School of Medicine, South China University of Technology, Guangzhou, China.

[3] Department of Nephrology, Shanxi Kidney Disease Institute, Second Hospital of Shanxi Medical University, Taiyuan, China.

[4] School of Public Health and Emergency Management, School of Medicine, Southern University of Science and Technology, Shenzhen, China.

[5] Guangdong Provincial Key Laboratory of Tumor Interventional Diagnosis and Treatment, Zhuhai People’s Hospital, Zhuhai Clinical Medical College of Jinan University, Zhuhai, China.

[6] Department of Pathophysiology, Shenzhen University Health Science Center, Shenzhen University, Shenzhen, China.

[7] Inflammation and Immune Mediated Diseases Laboratory of Anhui Province, Anhui Institute of Innovative Drugs, School of Pharmacy, Anhui Medical University, Hefei, China.

[8] Institute for Liver Diseases of Anhui Medical University, Hefei, China.

[9]These authors contributed equally to this work.

[10]Lead Contact.

***Corresponding author:**

Meixiao Zhan MD, PhD

Professor

Guangzhou First Pepople's Hospital, the Second Affiliated Hospital, School of Medicine, South China University of Technology, Guangzhou, 510006, China.

Guangdong Provincial Key Laboratory of Tumor Interventional Diagnosis and Treatment, Zhuhai People's Hospital, Zhuhai Clinical Medical College of Jinan University, Zhuhai, 510009, China.

Tel:+86-(020)81048319

Email: zhanmeixiao@ext.jnu.edu.cn

Yuliang Feng MD, PhD

Associate Professor

Department of Pharmacology, School of Medicine; Southern University of Science and Technology, Shenzhen, Guangdong, 518055, China.

Tel:+86 (755)-88012564

Email: fengyl@sustech.edu.cn

Tao Xu PhD

Professor

Inflammation and Immune Mediated Diseases Laboratory of Anhui Province, Anhui Institute of Innovative Drugs, School of Pharmacy, Anhui Medical University, Hefei, 230032, China.

Institute for Liver Diseases of Anhui Medical University, Hefei, 230032, China.

Tel: +86 (0551)-65172131

Email: xutao@ahmu.edu.cn

Wen Su MD, PhD

Associate Professor

Department of Pathophysiology, Shenzhen University Health Science Center, Shenzhen University, Shenzhen, 518071, China.

Tel:+86 18188610625

Email: suwen@szu.edu.cn

Keywords: Metabolic dysfunction-Associated fatty liver disease, Cardiovascular diseases, genome-wide association studies, Shared genetic architectures, Genetic pleiotropy.

Abstract: 275 words

Electronic word count manuscript: 4,568 words

Main figures and tables: 4 main figures, 1 main tables

Supplementary material: 2

Conflict of interest statement

All authors declare no competing interests.

Financial support statement

This study was supported by the Natural Science Foundation of China Excellent Young Scientists Fund (Overseas) (Grant no. K241141101), Guangdong Basic and Applied Basic Research Foundation for Distinguished Young Scholars (Grant no. 2024B1515020047), Shenzhen Pengcheng Peacock Plan, Shenzhen Basic Research General Projects of Shenzhen Science and Technology Innovation Commission (Grant no. JCYJ20230807093514029) (To Y.F.), Shenzhen University 2035 Program for Excellent Research 8690200000314, the Shenzhen Science and Technology Fund for Distinguished Young Scholars (RCYX20231211090127031) (to W. S.), National Natural Science Foundation of China (Grant no. 82230067, 82272103), the

Guangdong Provincial Key Laboratory of Tumor Interventional Diagnosis and Treatment (Grant no. 2021B1212040004), and the Natural Science Foundation of Guangdong Province of China (Grant no. 2022B1515020010) (To M.Z.), Shenzhen Science and Technology Program (Grant No. GJHZ20240218111401002 to J.B.), and Center for Computational Science and Engineering at Southern University of Science and Technology. The funder had no role in the design, implementation, analysis, interpretation of the data, approval of the manuscript, and decision to submit the manuscript for publication.

Author contributions

J.Q., M.C., M.C., Y.F., and M.Z. as conceptualization and supervised this project and wrote the manuscript. W.X., W.M., T.Y., Q.Z., and K.Y. performed the main analyses and wrote the manuscript. X.Y, Q.Y., J.X., and X.H. performed the statistical analysis and assisted with interpreting the results. W.S., T.X., Y.F., and M.Z. provided expertise in cardiovascular biology and GWAS summary statistics. All authors provided intellectual content and approved the final version of the manuscript.

Abstract

Background& Aims：Multiple epidemiological studies have suggested an association between Metabolic dysfunction-associated fatty liver disease (MAFLD) and cardiovascular diseases (CVDs). However, the genetic components that are shared between the two remain unclear.

Methods: This genome-wide pleiotropic association study integrated comprehensive genome-wide association studies (GWAS) summary data from publicly available sources within European populations. It employed a range of genetic approaches to analyze the shared genetic architectures between MAFLD and six CVDs: atrial fibrillation (AF), coronary artery disease (CAD), venous thromboembolism (VTE), heart failure (HF), peripheral artery disease (PAD), and stroke. Initially, we examined the genetic correlation and overlap between these conditions. Subsequently, Mendelian Randomization (MR) analysis was conducted to investigate potential causal relationships. Finally, we explored horizontal pleiotropy at the levels of single nucleotide polymorphisms (SNPs), genes, and biological pathways to further elucidate the shared genetic mechanisms underlying.

Results: We observed significant genetic associations between MAFLD and four CVDs, including CAD, HF, PAD, and VTE. However, we noted extensive genetic overlap in all but MAFLD-AF. MR analysis established causal relationships from MAFLD to both AF and PAD. Regarding horizontal pleiotropy, 49 pleiotropic loci were identified at the SNP level with functional annotations, 13 demonstrating strong evidence of colocalization. At the gene level, 14 unique pleiotropic genes were found ,

with SAMM50 (located at 22q13.31) being particularly notable. Further pathway enrichment analysis indicated that these genes significantly contribute to the pathway of establishment of protein localization to membrane, highlighting their pivotal role in the pathophysiology of both MAFLD and CVD.

Conclusions：In all, our research proved the shared genetic architectures and mechanisms between MAFLD and CVD and elucidated their shared genetic etiology and biological mechanisms.

Impact and implications

Metabolic dysfunction-associated fatty liver disease (MAFLD) has reached a prevalence of 25-30% worldwide and has emerged as a global leading cause of liver-related morbidity and mortality. Studies have shown that people with MAFLD have a higher risk of cardiovascular disease (CVD) than the general population and there is currently no effective drug to treat the comorbidity of the two, which imposes a burden on the socioeconomic situation and the adverse effects are still rising. Therefore, it is critical to understand how MAFLD affects CVD. Our study provides unique insights into the mechanisms of comorbidity between MAFLD and CVD. The increasing number of complications has prompted us to explore new treatment options, so our study has important clinical significance.

Graphical abstract

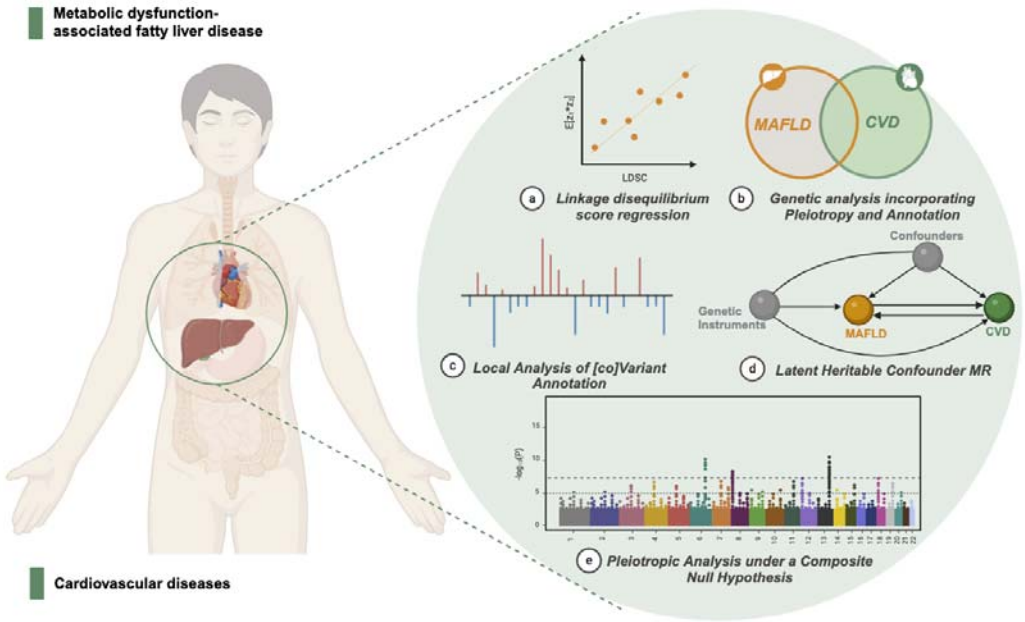

142

143

144 **Highlights:**

145 - The first comprehensive and systematic study to explore the common genetic
146 components between MAFLD and CVD.
147 - MAFLD and CVDs share genetic architectures and mechanisms.
148 - Genetically predicted MAFLD increases the risk of AF and PAD.
149 - The effects of *SAMM50* (located at 22q13.31) on lipid metabolism support the
150 comorbidity of MAFLD and CVDs.
151 - The localization of lipid droplet related contact site proteins to the membrane
152 plays a key role in the comorbidity of MAFLD and CVD.

Introduction

Non-alcoholic fatty liver disease (NAFLD) encompasses a range of liver disorders, from simple steatosis to non-alcoholic steatohepatitis, fibrosis, and cirrhosis, typically arising without significant alcohol consumption. According to a recent consensus statement by an international panel of experts, Metabolic dysfunction-Associated fatty liver disease (MAFLD) has been proposed as a more appropriate and comprehensive term to replace NAFLD, better reflecting its association with known metabolic dysfunctions[1,2]. MAFLD has emerged as a global leading cause of liver-related morbidity and mortality[3]. While liver-related complications significantly elevate mortality rates, cardiovascular diseases (CVDs) remain the primary cause of death in patients with MAFLD[4]. Clinically, individuals with MAFLD often exhibit elevated triglyceride levels and an increased concentration of residual lipoprotein particles, thereby elevating their risk for CVDs[5]. Lipoproteins containing apolipoprotein C3 (ApoC3) have been shown to activate the IL(interleukin)-1 to IL-6 to CRP (C-Reactive Protein) inflammatory pathway, which is implicated in the development of coronary artery disease (CAD), venous thromboembolism (VTE), Stroke, and vascular inflammation[6]. A meta-analysis of 16 observational studies, encompassing 34,043 patients over a median follow-up of 6.9 years, reported a 64% increased risk of fatal and/or non-fatal CVD events in patients with MAFLD compared to those without[7]. The strong epidemiological evidence underscores the association between MAFLD and an escalated risk of CVDs, which might suggest increased genetic liability to CVD in subgroups of patients with MAFLD.

Enhanced comprehension of the shared genetic foundations between MAFLD and various CVDs could offer valuable insights into these conditions. Recent large-scale genome-wide association studies (GWAS) have uncovered numerous risk loci linked to both MAFLD and CVDs, identifying several shared risk loci, notably at 19p13.11 (*TM6SF2*)[8] and 22q13.31 (*PNPLA3*)[9]. Increasing evidence suggests genetic overlap between MAFLD and CVDs. For instance, recent data suggested weak to moderate positive genetic correlations between MAFLD and CAD, heart failure (HF), and Hypertension, a major risk factor for CVDs[10]. Genetic correlation provides a summary measure of the correlation across all single-nucleotide polymorphism (SNP) effect sizes. However, it cannot differentiate between genetic overlap with a combination of concordant and discordant effects and a complete absence of genetic overlap, frequently resulting in an estimate close to 0 in both scenarios[11]. While genetic correlation can provide evidence for overall genomic similarity between traits, it does not provide information for considering biological plausibility or inferring potential causal relationships[12]. Previous Mendelian randomization(MR) analyses investigating the link between MAFLD and CVDs have shown that the causal relationship was not consistently robust due to possible bias by the presence of horizontal pleiotropy or sample overlap[13-15]. Despite these insights, a significant portion of the genetic underpinnings of MAFLD and CVDs remain elusive. Moreover, individual loci associated with both conditions have not been systematically analyzed, an examination of which could clarify the impact of different risk loci on the

comorbidities of MAFLD and CVDs, as well as identify biological pathways offering therapeutic promise.

This study aims to uncover their genetic overlap beyond the genetic correlation between MAFLD and six major CVDs—atrial fibrillation (AF), CAD, VTE, HF, peripheral artery disease (PAD), and Stroke—by leveraging unprecedentedly large GWAS summary data from European ancestry. We applied the genetic analysis incorporating pleiotropy and annotation (GPA), which estimates the total number of unique and shared genetic variants between pairs of traits. The relevance of mixed effects has been further emphasized by Local Analysis of [co]Variant Annotation (LAVA), which calculates local genetic correlations across the genome, even in the presence of minimal r_g. Given that GPA and LAVA quantify total genetic overlap but cannot pinpoint shared genomic loci, we subsequently utilized the Pleiotropic Analysis under a Composite Null Hypothesis (PLACO) method to discover loci jointly associated with MAFLD and each CVD beyond genome-wide significance, a critical step for gaining biological insights. Additionally, we also utilize Latent Heritable Confounder Mendelian randomization (LHC-MR) analyses to explore potential causal relationships between MAFLD and CVDs, considering sample overlap, bidirectional causal associations, and unobserved heritable confounders. Together, these methods augment the insights gained from genetic correlation analyses, shedding light on the distinct and common genetic frameworks underpinning MAFLD and CVDs, with implications for how we conceptualize

219 genetic risk for the comorbidity between MAFLD and CVDs.

220

221 **Materials and methods**

222 **Data sources and quality control**

223 Genetic associations with MAFLD were derived from the largest genome-wide
224 meta-analysis to date, involving 8,434 cases and 770,180 controls from four European
225 cohorts: the Electronic Medical Records and Genomics (eMERGE) Network, the UK
226 Biobank (UKB), the Estonian Biobank (EstBB), and the FinnGen Consortium, of
227 which the diagnosis was determined based on the electronic health records of all
228 participants[16]. To ensure that the sample size is large enough to produce reliable
229 results, we use GWAS summary data from studies with sample sizes greater than
230 50,000. Accordingly, our study encompassed six major CVDs, including AF, CAD,
231 VTE, HF, PAD, and Stroke. Specifically, GWAS summary statistics for AF were
232 retrieved from a recent meta-analysis of six cohorts, including the Health Study
233 Nord-Trøndelag (HUNT), deCODE, Michigan Genome Initiative (MGI), DiscovEHR,
234 UKB, and AFGen consortium, comprising 60,620 cases and 970,216 controls of
235 European ancestry[17]. GWAS summary statistics for CAD were extracted from a
236 genome-wide meta-analysis by the CARDIoGRAMplusC4D and UKB consortium,
237 including 181,522 cases and 984,168 controls of European ancestry[18]. GWAS
238 summary statistics for VTE were collected from the largest meta-analysis of seven
239 cohorts to date, including 81,190 cases and 1,419,671 controls of European ancestry[19].
240 GWAS summary data for HF were derived from the Heart Failure Molecular

Epidemiology for Therapeutic Targets (HERMES) consortium, entailing 47,309 cases and 930,014 controls[20]. GWAS summary data for PAD came from the largest meta-analysis conducted on data from 11 independent cohorts, totaling 12,086 cases and 499,548 controls[21]. GWAS summary data for Stroke were obtained from the GIGASTROKE consortium, which included 73,652 cases and 1,234,808 controls[22]. Detailed information about these GWAS summary data and their original publication sources is available in Supplementary Table 1.

Quality control was carried out strictly for GWAS summary data per the following steps before further analysis:(i) alignment with the hg19 genome assembly, and the 1000 Genomes Project v3 Europeans was used as the reference[23]; (ii) only including autosomal SNPs; (iii) SNPs with duplicate entries or missing rsIDs were eliminated; (iv) SNPs with a minor allele frequency (MAF) value of 0.01 or less were excluded. To ensure robust results, we normalized the GWAS summary data for all phenotypic SNPs, yielding 6,479,654 common SNPs across all diseases.

Assessing the genetic correlates of MAFLD and CVDs

We employed cross-trait linkage disequilibrium score regression (LDSC) analyses to assess the genetic correlation (r_g) between MAFLD and six major CVDs[24]. LDSC, an effective method for evaluating genetic correlations across the genome, utilizes the linkage disequilibrium (LD) structure to estimate individual SNP effect sizes from GWAS summary statistics[25]. The method involves regression of these GWAS summary statistics against LD scores derived from the European 1000 Genomes Project, minimizing biases related to polygenicity, sample overlap, and population

stratification[24]. Due to its complexity, the major histocompatibility complex (MHC) region was excluded from our analysis. First, univariate LDSC was conducted to determine the SNP-based heritability (h^2_{SNP}) for MAFLD and each CVD. Subsequently, bivariate LDSC estimated the r_g between MAFLD and CVDs by performing a weighted linear regression on the product of Z-scores for MAFLD and CVDs against the LD scores for all available genetic variants. This approach provides an unbiased estimate of r_g and reliably measures genetic correlations even in overlapping samples between GWAS datasets. Genetic correlations rang from -1 to +1, with values closer to the extremes indicating stronger influences, and negative values suggest opposite-direction effects, while positive values indicate the same direction. *P*-values below a Bonferroni-corrected significance threshold ($P = 0.05 / 6 = 8.3\times10^{-3}$) were considered statistically significant.

To identify tissues closely associated with genetic susceptibility SNPs for MAFLD and CVDs, we used LDSC applied to specifically expressed genes (LDSC-SEG)[26]. This method combines aggregate GWAS summary statistics with tissue-specific gene expression data for targeted tissue enrichment analysis[26]. Our analysis incorporated various gene sets, including multi-tissue gene expression data from the GTEx project (v8) and chromatin information from the Roadmap Epigenomics and ENCODE initiatives[26,27]. Using the baseline model and comprehensive gene sets, we prioritized genes from GTEx based on computed t-statistics, focusing on the top 10% of specifically expressed candidate genes that exhibited the highest t-statistics. The P-value from the regression coefficient's z-score was used to determine the significance coefficient, and a false discovery rate (FDR) of less than 0.05 was applied to assess the significance of enriched SNPs in specific tissues.

Estimating genetic overlap between MAFLD and CVDs

To address the "missing heritability" issue in complex traits, the Genetic Analysis incorporating Pleiotropy and Annotation (GPA) was specifically developed. This tool

was specifically designed to overcome the limitations posed by the small proportion of genetic variants identified through standard approaches that account for only a minimal part of the expected genetic contribution[28]. GPA achieves this by integrating diverse genomic data and annotation information, thereby enhancing the prioritization of GWAS results and providing a more comprehensive estimation of genetic overlap. Notably, in the absence of annotation data, GPA can infer genetic overlap using p-value interactions of the corresponding phenotypes[28]. GPA is based on key assumptions regarding p-value distributions: p-values from null SNPs are expected to adhere to a uniform distribution, reflecting no association, while p-values from non-null SNPs are presumed to follow a beta distribution, indicating potential associations. Within this framework, GPA categorizes SNPs into four groups based on their p-value characteristics: $\pi 00$ suggests no association with either trait; $\pi 01$ denotes an association exclusively with the first trait; $\pi 10$ signifies an association solely with the second trait; and $\pi 11$ represents an association with both traits. This classification can estimate $\pi 11 / (\pi 10 + \pi 11 + \pi 11)$, an important ratio indicator that represents the proportion of SNPS shared by two traits, suggesting the extent to which a common biological pathway may be shared between the two traits[28]. Subsequently, the likelihood ratio test (LRT) was used to assess the statistical significance of the observed genetic overlap[28]. Given the complex interrelations among SNPs, GPA estimates are susceptible to biases from LD. We used PLINK1.9 for LD pruning to address this, drawing on data from the 1000 Genomes Project Phase 3[23] for European ancestry. We also applied a Bonferroni-corrected significance threshold for multiple comparisons, set at $P = 0.05$ / number of trait pairs = $0.05 / 6 = 8.3 \times 10^{-3}$.

Calculating local genetic correlations between MAFLD and CVDs

LAVA facilitates the assessment of local genetic correlations by partitioning the genome into smaller regions, which enables detailed insights into the influence of genetic variants on various traits at a regional level, rather than across the entire genome[29]. LAVA analyses genetic correlations within different genomic segments,

using the regions delineated by Werme et al. as autosomal LD blocks[29], characterized by minimal connectivity between blocks. The genome was partitioned into 2,495 semi-independent regions, each approximately 1 Mb, using genotype data from the 1000 Genomes Project Phase 3 European ancestry as the LD reference panel and MHC region (chr 6: 25-35 Mb) was excluded. In conducting the genetic association study, we first performed a preliminary univariate analysis using LAVA to estimate the local heritability of MAFLD and CVDs. With this step, we could identify regions that showed significant signals in the local genetic analysis. We then performed bivariate LAVA analyses of these regions to explore regional genetic associations between MAFLD and CVDs. To ensure the statistical significance of the results, the FDR method was employed to calculate the adjusted p-value. FDR less than 0.05 was considered the genetic correlation of these regions to be statistically significant.

Evaluate the causal relationship between MAFLD and CVDs

The genome-wide and local genetic correlations provide insights into the shared genetic basis between trait pairs, but these correlations do not imply causality in either direction. To overcome these limitations, linkage disequilibrium heterogeneity causal Mendelian randomization (LHC-MR) provides a more refined approach to assess bidirectional causality while minimizing confounding effects[30]. This method extends traditional MR by addressing limitations of the standard two-sample MR approach, such as potential sample overlap, under-utilization of genome-wide markers, and the need to understand exposure-outcome relationships. LHC-MR assesses bidirectional causality by categorizing associations between exposure and outcome into four categories: (i) causal effect of exposure on outcome, (ii) causal effect of outcome on exposure, (iii) effect of confounders whose exposure affects the outcome process

(vertical pleiotropy), and (iv) effect of confounders whose exposure affects the outcome independently (horizontal pleiotropy[30]). Unlike traditional MR, LHC-MR utilizes all genome-wide genetic variation rather than only genome-wide significant variation[30]. To ensure the stability of the results, the Bonferroni correction significance threshold was set at 4.17×10^{-3} ($P = 0.05$/number of trait pairs/number of tests). When $P_{axy} < 4.17\times10^{-3}$ and $P_{ayx} > 0.05$, it suggests a one-way causal relationship from MAFLD to CVD; conversely, when $P_{ayx} < 4.17\times10^{-3}$ and $P_{axy} > 0.05$, it implies a one-way causal relationship from CVD to MAFLD. However, if both P_{axy} and P_{ayx}, exceeding the significance threshold, it indicates bidirectional causality between MAFLD and CVD. We used traditional two-sample MR techniques for sensitivity analysis, including Inverse Variance Weighting (IVW), MR Egger, Weighted Median, Simple Mode, and Weighted Mode. *P*-values below the 0.05 threshold were considered statistically significant.

Identification of pleiotropic loci between MAFLD and CVDs

To unravel the shared genetic mechanisms between MAFLD and six major CVDs, our study employs the PLACO, extending pleiotropic analysis to the SNP level[31]. PLACO utilizes the summary statistic from GWAS to calculate the test statistic for the product of the Z-statistics for each SNP in the two trait analyses. This calculation is based on the assumption of a mixed distribution, which allows for the assessment of SNP associations across traits. Using this assumption, PLACO can rigorously analyze individual SNPs by pairwise Z-statistics, categorizing the null hypothesis of

pleiotropy into three distinct and mutually exclusive scenarios: (i) H00, indicating no association of the SNP with either trait; (ii) H10, signifying an association with the first trait but not the second; and (iii) H01, representing an association with the second trait but not the first. The rejection of the composite null hypothesis, which encompasses all three scenarios, indicates horizontal pleiotropy, suggesting that the SNP influences both traits through identical mechanisms. We applied a stringent significance threshold of 5×10^{-8} to identify SNPs exhibiting statistically significant pleiotropy.

Functional annotation based on pleiotropic loci

To identify and conduct independent genomic loci between MAFLD and six major CVDs, we utilized the Functional Mapping and Annotation (FUMA) platform[32]. FUMA, an online tool designed to enhance the interpretability of GWAS findings, performs functional annotation of pleiotropic SNPs revealed by PLACO analysis. Lead SNPs are merged to delineate distinct genomic loci in LD blocks within 500 kb of lead SNPs by FUMA, utilizing default parameters and LD data from the 1000 Genomes Project Phase 3 European cohort. Lead SNP was further selected by $r^2 < 0.1$ for minimal LD in independent significant SNPs (genome-wide significance $P < 5\times10^{-8}$ and $r^2 < 0.6$), indicating higher independence from adjacent genetic variations. Despite these regions potentially containing several lead SNPs, the Top Lead SNP is identified with the lowest P-value within a given region. Locus was deemed novel to MAFLD and CVD if they did not coincide with the loci previously reported in the

392 original GWAS.

393

394 Functional annotations for Top Lead SNPs, provided by FUMA, include Combined
395 Annotation-Dependent Depletion (CADD[33]) scores, regulatory function probability
396 scores via RegulomeDB (RDB[34]), and potential effects on gene function as annotated
397 by ANNOVAR[35]. CADD scores, which assess the harmful impact of SNPs, are
398 utilized with a threshold: a score greater than 12.37 is considered likely to be harmful,
399 reflecting the SNP's potential to affect biological functions adversely. RDB scores,
400 ranging from 1 to 7, indicate the likelihood of an SNP being located in a regulatory
401 function area, with lower scores denoting higher functional significance. Lead SNPs
402 were annotated using ANNOVAR to evaluate their proximity to genes and potential
403 impacts on gene functions, thus providing insights into how these variants might
404 influence genetic pathways or disease mechanisms. For the identification of putative
405 causal genes, SNPs were mapped using two approaches: positional mapping within a
406 10-kb window around the SNP and eQTL mapping.

407

408 **Colocalization analysis**

409 After annotating pleiotropic loci using FUMA, we analyzed colocalization with the
410 "COLOC" R package to identify potential shared causal variants across trait pairs
411 within each locus. COLOC analysis employs Bayes factors to evaluate the likelihood
412 of shared causal variation between two sets of trait-associated loci, calculating
413 posterior probabilities (PP) for five mutually exclusive hypotheses at each locus: (i)

no SNP is associated with either trait (H0); (ii) a causal SNP is associated only with the first trait (H1); (iii) a causal SNP is associated only with the second trait (H2); (iv) each trait is influenced by independent, distinct causal SNPs (H3); and (v) a single SNP acts as a causal variant for both traits (H4). Our analysis primarily focuses on hypothesis H4, which posits a shared causal variant for both traits. Strong evidence of colocalization at a genomic locus is indicated if the posterior probability for shared causal variants (PPH4) exceeds 0.70. The SNP with the highest PPH4 within these loci is identified as the candidate causal variant.

Gene-level annotation analysis

To pinpoint genes that exhibit pleiotropic effects within genomic loci, a Multi-marker Analysis of GenoMic Annotation (MAGMA) was performed based on the results of PLACO and individual GWAS[36]. MAGMA, a tool rooted in multivariable regression models, computes the significance of gene-trait associations by incorporating principal component analysis. It then employs the F-test to ascertain p-values for each gene, considering factors such as gene size, SNP count per gene, and LD among the markers. Consistency in gene-based testing was ensured by defining gene boundaries, which encompassed regions extending ±10 kb from the termini of each gene. We obtained MAGMA gene IDs and location data for 17,636 protein-coding genes, aligning SNP locations with Human Gene Build 37 (GRCh37/hg19). The MHC region (chr6: 25-35 Mb) was excluded from MAGMA's gene-based analysis. Significant gene associations were identified using a stringent Bonferroni-corrected

436 threshold set at $P = 4.73\times10^{-7}$ (0.05 / 17,636 / 6), accounting for the number of
437 protein-coding genes and trait pairs analyzed.
438
439 Recognizing that MAGMA links SNPs to genes based primarily on physical
440 proximity, we extended our analysis to include the eQTL-informed MAGMA
441 (e-MAGMA)[37]. The e-MAGMA utilizes tissue-specific eQTL data to assign risk
442 variants to presumptive genes, thereby converting genome-wide association summary
443 statistics into gene-specific metrics. This method leverages tissue-specific eQTL data
444 from the GTEx project to account for long-range regulatory effects, enhancing the
445 interpretation of GWAS association signals. MHC region (chr6: 25-35 Mb) was
446 excluded in e-MAGMA analysis results as well as MAGMA to avoid confounding
447 due to complex LD patterns. Our study utilizes the GTEx v8 comprehensive database
448 containing eQTL data from 47 different tissues, based on PLACO results, to delve
449 into gene-disease associations at a fine-grained tissue level, and to gain a more
450 detailed understanding of the tissue-specific genetic architecture behind the relevant
451 diseases. To minimize confounding factors associated with broad tissue analyses, we
452 refined our approach by selecting a subset of tissues based on insights from
453 LDSC-SEG results and previous research. Specifically, our focused analysis included
454 ten tissues: two types of adipose tissue (subcutaneous and visceral omental fat), three
455 arterial tissues (aorta, coronary, and tibial arteries), two cardiac tissues (left ventricle
456 and atrial appendage), as well as liver, EBV-transformed lymphocytes, and whole
457 blood. Using the 1000 Genomes Project v3 European samples as the LD reference, we

458 calculated tissue-specific p-values for each gene across the selected tissues. We
459 applied a Bonferroni correction to determine the significance of these p-values,
460 accounting for the number of tissue-specific protein-coding genes and trait pairs
461 examined. For instance, the significance threshold for adipose subcutaneous tissue
462 was set at $P = 0.05 / 7{,}560 / 6 = 1.10 \times 10^{-6}$.
463
464 To further explore tissue-specific gene-trait associations for MAFLD and CVDs, we
465 conducted a transcriptome-wide association study (TWAS) using single-trait GWAS
466 results[38]. Employing the FUSION framework, TWAS integrates GWAS summary
467 statistics with eQTL data from the GTEx v8 dataset to assess how variations in gene
468 expression across specific tissues influence phenotypes. We used pre-computed gene
469 expression weight references from the tissues analyzed in our e-MAGMA study. LD
470 pruning was performed during the third phase of the 1000 Genomes Project using the
471 LD structures of the European subpopulation. Significance thresholds were adjusted
472 using tissue-specific Bonferroni corrections to control for multiple tests.
473
474 **Pathway level analyses**
475 We performed functional enrichment analysis on the overlapped gene lists
476 significantly identified by MAGMA and e-MAGMA analyses using the ToppGene
477 functional annotation tool (ToppFun)[39]. ToppGene Suite is a comprehensive portal for
478 gene list enrichment analysis and candidate gene prioritization. The ToppFun
479 application provides a variety of annotation data types, including transcriptome,

480 proteome, regulatory elements (such as transcription factor binding sites (TFBS) and
481 microRNA), ontologies (such as GO and Pathway), phenotypes (including human
482 diseases and mouse phenotypes), pharmacometrics (drug-gene associations), and
483 literature co-citations. Additionally, ToppFun prioritizes candidate genes based on
484 their functional similarity to ensure rigorous and thorough analysis. Significant GO
485 terms were identified with an FDR threshold of 0.05.
486

487 **Results**

488 **SNP-based heritability and genetic correlations between MAFLD and CVDs**

489 After harmonizing and filtering SNPs common across GWAS summary statistics,
490 LDSC was utilized to estimate the h^2_{SNP} and the genome-wide genetic correlations (r_g)
491 between MAFLD and CVDs. Univariate LDSC analysis indicated that the h^2_{SNP} of
492 MAFLD was 0.002 (SE = 0.001). In comparison, the h^2_{SNP} of CVDs ranged from
493 0.008 to 0.032, with CAD exhibiting the highest heritability (h^2_{SNP} = 0.032, SE =
494 1.90×10^{-3}) and HF the lowest (h^2_{SNP} = 0.008, SE = 3.01×10^{-3}). Notably, the
495 heritability of MAFLD was lower than that of any individual CVD. Bivariate LDSC
496 revealed that all trait pairs exhibited positive genetic correlations under a relaxed
497 significance threshold (P < 0.05). However, four trait pairs maintained statistical
498 significance after applying a Bonferroni correction for multiple comparisons (P <
499 $0.05 / 6 = 8.33\times10^{-3}$). These findings highlight the subtle genetic interactions between
500 MAFLD and CVD, which underscores the potential for shared genetic pathways to
501 influence these complex diseases.

502

503 **Genetic overlap analysis**

504 The r_g is a vital metric that reflects the genetic relationship between trait pairs,
505 providing insights into their shared genetic architecture. Importantly, a r_g value close
506 to zero does not necessarily signify the absence of a genetic association between traits.
507 This apparent discrepancy can arise from various factors, such as the mixed effects of
508 homozygosity and reverse effects, or a lack of genetic overlap, which may mask the
509 true genetic relationships and lead to misleadingly low r_g values. Recognizing this
510 limitation highlights a "missing dimension" in our understanding of genetic
511 connections between phenotypes. To enhance our understanding of genetic
512 interactions and address these challenges, advanced statistical methods, including
513 GPA and LAVA, have been employed by us.

514

515 The intricacies of the genetic relationships observed between MAFLD and CVDs,
516 particularly the surprising contrast between significant genetic overlap and weak
517 correlation in some cases, underscore the complexity of genetic interactions and the
518 importance of considering additional analytical dimensions. In our analysis of six trait
519 pairs, the MAFLD-AF pair was the only one that failed to meet the Bonferroni
520 correction threshold, indicating a lack of significant genetic overlap. Conversely, the
521 MAFLD-CAD pair demonstrated the most significant genetic overlap, evidenced by a
522 P-value of 7.12×10^{-31}, aligning with LDSC results, which revealed the highest genetic
523 correlation (r_g = 0.627, P = 5.18×10^{-6}). Although a significant genetic overlap was

identified between MAFLD and Stroke ($P = 6.96\times10^{-6}$), the minimal PAR value (PAR = 7.00×10^{-4}) highlights a small proportion of pleiotropic SNPs. Furthermore, the weak genetic correlation between MAFLD and Stroke ($r_g = 0.627$, $P = 3.98\times10^{-2}$) suggests that the presence of multiple closely linked SNPs with independent or heterogeneous impacts may obscure consistent effects, resulting in a correlation that falls short of higher statistical confidence thresholds. This phenomenon, where broad genetic overlap coexists with weak genetic correlation, implies that mixed effects may mask the true genome-wide genetic correlation.

Regional genetic correlation analysis

LAVA evaluates genetic correlations within specific genomic regions and identifies subtle genetic effects that might elude detection by LDSC. This capability is vital, as genetic influences often vary across the genome, and the correlations between traits can differ markedly by region. First, a univariate LAVA analysis was conducted by us with a strict threshold of $P < 1\times10^{-4}$ to identify regions with strong genetic signals, resulting in the identification of 2,336 significant regions. These regions were then formed into 77 bivariate test sets for more detailed analysis. In the subsequent bivariate LAVA analysis, we applied a looser significance threshold ($P < 0.05$), identifying approximately 22 genomic regions showing genetic signals associated with all trait pairs. Notably, our LAVA analysis revealed five key genetic regions associated with MAFLD and stroke, including three negatively and two positively correlated regions. This discovery of substantial genetic overlap starkly contrasts the

546 lack of significant genome-wide associations found using LDSC. This discrepancy
547 between the LAVA and LDSC results underscores the complex genetic architecture,
548 suggesting that regions with both positive and negative correlations may lead to a
549 heterogeneous distribution of genetic effects. Such complexity might mask genetic
550 signals when assessed on a genome-wide scale using LDSC. We then applied a
551 stricter threshold of $P < 6.49\times10-4$ to account for multiple comparisons. This led to
552 the identification of a significant region on chromosome 8, spanning from
553 125,453,321 to 126,766,827, showing a strong correlation between MAFLD and CAD
554 ($r_g s$=0.509, P =3.05×10^{-6}), aligns with the positive genetic correlation observed across
555 the genome by LDSC.
556

557 **Causal relationship linking MAFLD and CVDs**

558 The observed genetic overlap between MAFLD and CVDs extends beyond mere
559 correlation, suggesting the presence of pleiotropy. However, determining whether this
560 pleiotropy is horizontal or vertical remains unresolved. To clarify this, we utilized the
561 LHC-MR approach, which sheds light on the bidirectional causal relationships
562 between MAFLD and CVD through vertical pleiotropy. Our findings revealed a
563 significant positive causal effect of MAFLD on both AF and PAD, with odds ratios
564 (OR) of 1.11 (P = 2.36×10^{-3}) and 1.375 (P = 1.39×10^{-4}), respectively. These results
565 underscore MAFLD as a critical risk factor in the onset and development of both AF
566 and PAD, aligning with previous research that highlights MAFLD's role in increasing
567 the prevalence of these disorders. Notably, we found no evidence to suggest reverse

causality in these relationships.

Shared variants and functional annotation of MAFLDs and CVDs

To further dissect the complex genetic mechanisms between MAFLD and CVDs, we utilized PLACO to identify significant pleiotropic variants indicative of horizontal pleiotropy. This inquiry, through its meticulous analysis, unveiled a trove of 3,438 SNPs exhibiting significant pleiotropic influences. Subsequently, these SNPs underwent a process of annotation, facilitated by the FUMA tool, which meticulously delineated 49 distinct loci spanning 20 chromosomal regions, enriching our understanding of the genetic landscape under scrutiny. Seven of the 49 loci identified were novel and had not been previously associated with MAFLD or CVDs. Among the 22 loci (44.9%), the selected effect alleles at the top SNPs within or near loci demonstrated effect directions that were consistent with each other which means they may concurrently increase ADs and CVDs or diminish the risk of developing ADs and CVDs. Notably, three loci, 22q13.31, 16q12.2, and 8q24.13, were associated with more than half of the trait pairs analyzed. The chromosomal region 22q13.31, in particular, is implicated in five trait pairs, excluding MAFLD-Stroke, highlighting its significance in the pleiotropic landscape. For example, *SAMM50* located at 22q13.31, studies have shown that *SAMM50* gene polymorphisms are associated with the occurrence and severity of fatty liver disease, which may be related to reduced fatty acid oxidation caused by *SAMM50* deficiency[40]. Although there is no direct evidence linking *SAMM50* to cardiovascular disease, its potential effects on heart development

and function by regulating mitochondrial autophagy may influence cardiovascular disease risk[41]. Moreover, the *FTO* gene, located in the 16q12.2 region, is another gene of interest due to its impact on energy intake and expenditure, potentially increasing susceptibility to both MAFLD and CVDs[42,43]. Moreover, the *TRIB1* gene, located at 8q24.13, plays a critical role in regulating lipid metabolism. It influences downstream signaling pathways such as PI3K-AKT and MAPK, which promote the accumulation of liver lipids and increase the risk of MAFLD[44,45]. Additionally, polymorphisms in the *TRIB1* gene have been linked to an increased risk of CAD and Stroke. Specifically, the A allele at rs2954029 has been significantly associated with these conditions; individuals carrying the A allele exhibit a higher risk of both CAD and stroke[46].

Functional annotation via FUMA identified 24 intronic SNPs, 14 intergenic SNPs, and 5 exonic SNPs. For example, the 22q13.31 region includes the exonic SNP rs1007863, which showed significant eQTL associations in several tissues: adipose subcutaneous ($P = 2.38\times10^{-6}$), adipose visceral omentum ($P = 2.16\times10^{-15}$), whole blood ($P = 3.57\times10^{-5}$), artery aorta ($P = 3.57\times10^{-5}$), and artery tibial ($P = 1.42\times10^{-12}$). Notably, the P-value for adipose visceral omentum was used as the P-value for this region in MAFLD-AF for PLACO results, indicating that this P-value is considered the most appropriate or representative indicator, suggesting that visceral tissues are importantly associated with this trait pair. Seven of all pleiotropic SNPs were identified as potentially deleterious, with a CADD score greater than 12.37. Notably, rs28929474 exhibited the highest CADD score of 20.2, suggesting its potential

association with the development of MAFLD and CAD and its deleterious effects. Furthermore, based on RDB scores, two SNPs were found to potentially impact transcription factor binding, with rs10401969 showing the most significant effect (RBD = 1f). Further colocalization analysis revealed evidence of colocalization in 13 of the 49 pleiotropic loci (PPH4 > 0.7). Notably, the 16q12.2 region has demonstrated a robust colocalization signal across all four trait pairs it encompasses (with a posterior probability of heterogeneity, PPH4, ranging from 0.766 to 0.890).

Gene-level annotation of MAFLD and CVDs

Using MAGMA, we identified 34 potential pleiotropic genes (28 of which are unique) between MAFLD and CVDs after Bonferroni correction, which is situated on or overlaps with 49 previously identified pleiotropic loci. Among these, 2 are novel unique genes, 3 have newly unique been associated with CVDs, and 23 are newly unique implicated in MAFLD. Notably, three genes—*SAMM50*, PNPLA3, and *FTO*—were detected in two or more trait pairs. Further, of the genes identified by MAGMA, 32 were corroborated by FUMA's locus mapping. The pervasive impact of *SAMM50* across multiple traits underscores its significance and makes it a primary focus of our ongoing investigation.

We performed tissue-specific analyses employing LDSC-SEG to identify the tissues associated with each disease. After adjusting for multiple comparisons using the FDR method, significant associations were observed solely with CVDs. Specifically, for AF,

the auricle and the left ventricle were identified as the primary tissues driving the condition, suggesting that functional changes in these areas may play a crucial role in its development and maintenance. Similarly, in CAD, the predominant tissues associated with the disease were located in arterial regions, including the aorta, coronary artery, and anterior tibial artery, with the anterior tibial artery demonstrating the most significant impact. Unfortunately, while MAFLD showed enrichment in the anterior cingulate cortex, cerebral cortex, and frontal cortex, these did not meet the significant threshold for correction. In all, afte integrating the results of tissue enrichment analysis with tissues commonly implicated in clinical practice for these conditions, we finally selected 10 tissues for subsequent analysis.

Given the limitations of MAGMA, which assigns SNPs based solely on proximity to genes and may overlook the effects of distant gene regulation, we employed e-MAGMA to overcome these deficiencies. By integrating eQTL data from 10 distinct tissues, e-MAGMA enabled us to identify 161 tissue-specific genes, including 59 that were unique. Notably, *IRAK1BP1*, *ATP13A1*, *SAMM50* and *NME7* were identified in more than half of the trait pairs. *IRAK1BP1* exhibits high specificity to nine tissues except EBV-transformed lymphocytes and has not previously been associated with MAFLD or any CVDs. However, its involvement in inflammation suggests a potential role in these diseases. Our findings were further validated using FUMA's GTExV8 data through e-MAGMA, confirming the identification of 78 tissue-specific genes, including *SAMM50* at 22q13.31. Subsequent TWAS analysis of

656 the original GWAS results was used to validate the EMAGMA analysis, and 300
657 tissue-specific genes were identified as new genes for MAFLD and 185 as new genes
658 for CVDs.
659
660 Finally, 17 pleiotropic genes (14 unique) were identified by MAGMA and e-MAGMA.
661 *SAMM50* at 22q13.31 was the only gene that appeared in multiple trait pairs (except
662 for MAFLD-PAD and MAFLD-Stroke), while other genes appeared only in single
663 trait pairs.
664
665 **Functional enrichment analysis of pleiotropic genes in MAFLD and CVDs**
666 Understanding how identified genes collectively fulfill specific biological functions
667 through shared pathways enhances our ability to derive meaningful interpretations
668 from genomic data. The tool ToppFun assists in mapping these genes to their
669 respective enrichment pathways and biological processes, which can reveal the
670 activity levels or enrichment of certain pathways. Notably, three pathways were
671 significantly enriched: membrane organization, endoplasmic reticulum tubular
672 network organization, and the establishment of protein localization to the membrane.
673 Protein localization is critical in the accumulation of lipid droplets near mitochondria;
674 it helps protect mitochondrial function by sequestering toxic lipids. This protective
675 mechanism is crucial for managing lipid accumulation in the liver and other tissues,
676 where excessive lipid buildup can lead to MAFLD and CVDs[47,48]. Proper protein
677 localization, therefore, plays a pivotal role in mitigating lipid toxicity and maintaining

678 cellular balance, thereby reducing the risk of both MAFLD and CVD.

679

680 **Discussion**

681 This genome-wide pleiotropic association study offers compelling evidence of a
682 shared genetic architecture and mechanisms between MAFLD and six major CVDs.
683 We observed moderate to strong genome-wide genetic associations between MAFLD
684 and four CVDs—CAD, HF, PAD, and VTE—with notable genetic overlap in all but
685 the MAFLD-AF trait pair. MR analysis provided evidence of causal relationships for
686 two trait pairs, underscoring the presence of vertical pleiotropy. Additionally, at the
687 SNP level, our cross-trait analysis pinpointed 49 pleiotropic loci, 13 demonstrating
688 strong evidence of colocalization. Further analysis at the gene level through MAGMA
689 and e-MAGMA identified 45 (34 unique) significant position-specific pleiotropic
690 genes and 161 (59 unique)tissue-specific pleiotropic genes, including 17 overlapping
691 pleiotropic genes (14 unique because *SAMM50* was identified in 4 trait pairs).
692 Moreover, at the biological pathway level, protein localization to membrane signaling
693 pathways was identified as potentially pivotal in the co-pathogenesis of MAFLD and
694 CVD. These insights not only deepen our understanding of their intertwined genetic
695 etiology but also illuminate potential targets for therapeutic intervention and
696 preventive strategies.

697

698 In our study, bivariate LDSC revealed extensive positive genetic correlations between
699 MAFLD and six major CVDs, among which only four trait pairs (including

MAFLD-CAD, MAFLD-HF, MAFLD-PAD, and MAFLD-VTE) passed the Bonferroni correction. Further analysis using the GPA method demonstrated significant genetic overlap for all pairs except MAFLD with AF, underscoring the shared genetic underpinnings of these conditions. Interestingly, although no significant genome-wide genetic correlation was detected between MAFLD and stroke, substantial genetic overlap suggested the presence of complex genomic interactions, which was also confirmed by local genetic correlations of LAVA. In the MAFLD-stroke pair, we identified loci with mixed effect directions—two positively and three negatively correlated—suggesting that local mixed effects might underlie the non-significant genome-wide genetic correlation, potentially driven by a range of pleiotropic variants[11]. Additionally, despite the lack of a significant association between MAFLD and AF in both LDSC and GPA analyses, our bivariate LAVA under a loose threshold indicated a positive regional genetic correlation between the two. Overall, our findings confirm that MAFLD and CVDs share substantial heritability and genetic components, elucidating the genetic basis of their high comorbidity.

The shared genetic basis between MAFLD and CVD is primarily driven by horizontal and vertical pleiotropy (i.e., causal relationships). We employed the LHC-MR method to investigate potential causal links between MAFLD and 6 major CVDs. Our analysis revealed that genetically predicted MAFLD is causally associated with an increased risk of AF and PAD. These findings are consistent with prior epidemiological evidence. A meta-analysis confirmed an association between

MAFLD and an increased risk of AF[49]. Concurrently, a separate cohort study observed a high prevalence of PAD among MAFLD patients over 40 years old in the United States during a 13-year follow-up[50]. Conversely, we found no established causal relationship between MAFLD and HF or Stroke, nor was a reverse causal relationship between MAFLD and CVD supported. This contrasts with earlier MR analyses that reported a positive causal relationship between MAFLD and both HF[15] and CAD[14], which suggested a 15% increase in CAD incidence per unit increase in MAFLD. These discrepancies may arise from limitations in previous studies, such as potential genetic confounders and smaller sample sizes, which could impact the reliability of the exposure-outcome relationship. LHC-MR analysis is particularly effective at generating potential causal effects by excluding confounding factors, even in the face of unmeasured confounding. Leveraging extensive sample data and advanced methodologies, our study provided more robust and reliable causal effect estimates. Our study only provides partial evidence for vertical pleiotropy, suggesting that the shared genetic basis between MAFLD and CVD is primarily driven by horizontal pleiotropy.

Horizontal pleiotropy analysis further elucidated the common genetic architecture between MAFLD and CVD by discovering pleiotropic variants and loci, pleiotropic genes, and biological pathways between the two. Further investigation through horizontal pleiotropy analysis has confirmed their extensive comorbidity, identifying widespread pleiotropic variants across several key loci, such as 22q13.31, 16q12.2,

and 8q24.13, which are prominently associated with more than half of the trait pairs analyzed. Notably, the locus at 16q12.2—associated with all trait pairs except MAFLD-CAD and MAFLD-Stroke—maps to the *FTO* gene. This gene plays a critical role in lipid metabolism by enhancing oxidative stress and increasing lipogenesis in hepatocytes, thereby exacerbating MAFLD progression[51]. Moreover, according to a meta-analysis of 10 observational studies (19,153 CVD cases and 103,720 controls), variants in the *FTO* gene have been shown to significantly elevate CVD risk, independent of BMI and other conventional risk factors[52]. Moreover, in a large prospective longitudinal study of Type 2 diabetes (T2D) patients, variants in the *FTO* gene were also found to increase the risk of myocardial infarction and cardiovascular death by influencing a dyslipidemic phenotype typical of insulin resistance[53]. The above evidence suggests that the lipid metabolism process can be significantly changed by affecting the expression of the *FTO* gene, thereby improving MAFLD and reducing the risk of cardiovascular death.

In our gene-level analysis using MAGMA and e-MAGMA, we identified significant pleiotropic genes at the 22q13.31 locus, including patatin-like phospholipase-domain containing protein 3 (*PNPLA3*) and sorting and assembly machinery component 50 (*SAMM50*). These genes play crucial roles in the comorbidity between MAFLD and CVDs. *PNPLA3*, which exhibits weak hydrolytic activity towards glycerolipids, has been linked to the development of MAFLD and CVDs, excluding PAD and Stroke. This gene is associated with a missense variant closely linked to triacylglycerol (TAG)

accumulation in the liver—a major genetic risk factor for steatotic liver diseases[54,55]. *PNPLA3* competitively displaces adipose triglyceride lipase (ATGL) from lipid droplets, reducing lipolytic activity and promoting the progression of MAFLD[54]. Intriguingly, a GWAS meta-analysis revealed that the *PNPLA3* G-allele rs738409 offers modest protection against CAD by reducing triglyceride breakdown in the liver, thus affecting the secretion of very low-density lipoprotein particles and the development of atherosclerosis[56]. Additionally, our e-MAGMA analysis identified *SAMM50* at this locus as influencing most trait pairs. As an essential component of the Sorting and Assembly Machinery (SAM) complex on the outer mitochondrial membrane, *SAMM50* is vital for β-barrel protein biogenesis and interacts directly with the translocator of the outer mitochondrial membrane (TOM) complex[41]. It plays a significant role in fatty acid β-oxidation and, when deficient, can lead to intracellular lipid accumulation, exacerbating MAFLD[40]. Moreover, *SAMM50*'s involvement in mitochondrial dysfunction may impair the removal of reactive oxygen species (ROS), further contributing to the progression of MAFLD[57] and increasing susceptibility to HF by impairing mitochondrial function[41]. This mitochondrial pathway regulated by *SAMM50* offers a theoretical basis for the observed comorbidity between MAFLD and HF in our study, underscoring the potential for targeted therapies at this genetic locus.

In our pathway-level analysis, we discovered a crucial role for the gene *SAMM50* in mediating protein localization to membranes, a process integral to the pathogenesis of

MAFLD. This protein localization is especially important in how lipid droplets accumulate near mitochondria, which may protect mitochondrial function by sequestering toxic lipid species. Proteins that migrate to these lipid droplets at membrane contact sites are prime candidates for facilitating this protective mechanism[47,48]. In the liver, an excessive influx of lipids leads to the accumulation of triglyceride (TG)-rich lipid droplets, a hallmark of MAFLD[47]. Variations in genes associated with lipid droplet formation, such as PNPLA3, acting as both phospholipase and acyl transfer enzyme, is an important regulating factor for TG. It limits the activity of triglyceride hydrolases, leading to TG accumulation in the liver, thus predisposing to MAFLD[58]. Moreover, when lipid droplets amass in peripheral organs, the overflow of toxic lipids can contribute to CVDs. ATGL plays a pivotal role in this context by hydrolyzing TG within these droplets. It activates the PPARα/peroxisome proliferator-activated receptor-γ coactivator 1 (*PGC1*) complex in cardiomyocytes. A deficiency in cardiac ATGL leads to reduced *PGC1* expression, resulting in mitochondrial dysfunction and lipid accumulation, which can progress to HF[59]. In conclusion, the localization of contact site proteins related to lipid droplets is instrumental in preventing lipid overflow and safeguarding mitochondrial function. This mechanism significantly reduces the risk of both MAFLD and CVD by maintaining crucial cellular balances and interactions.

Our study has several limitations. First, our study population was confined to individuals of European ancestry, necessitating further research across other ethnic

groups to determine the universal applicability of our findings. Second, the datasets used for MAFLD and CVD included some cases with existing or potential co-morbid conditions, which may have biased our investigation of genetic overlap. Third, our analysis was limited to common genetic variants, highlighting the need for future studies to explore the impact of rare variants, which may also significantly influence the high comorbidity observed between MAFLD and CVD. Finally, while we reported some statistically significant findings, further investigation is required to assess their clinical relevance and implications.

In summary, our study demonstrates extensive genetic overlap, partial genetic correlation, and causal relationships between MAFLD and six major CVDs. Identification of the pleiotropic gene, *SAMM50*, at pleiotropic risk loci 22q13.31, shared between MAFLD and CVD, suggesting a common biological mechanism, namely the establishment of protein localization to the membrane, uncovering indications of shared genetic foundation for MAFLD and CVDs. This research enhances the shared genetic map of these diseases and offers new perspectives on preventing and treating their co-morbidities.

Abbreviations

AF (atrial fibrillation) ApoC3 (apolipoprotein C3) ATGL (adipose triglyceride lipase) CVDs (cardiovascular diseases) CAD (coronary artery disease) CRP (C-Reactive Protein) CADD (Combined Annotation-Dependent Depletion) e-MAGMA (eQTL-informed MAGMA) eMERGE (Electronic Medical Records and Genomics) EstBB (Estonian Biobank) FUMA (Functional Mapping and Annotation) FDR (false discovery rate) GPA (Genetic Analysis incorporating Pleiotropy and Annotation) GWAS (genome-wide association studies) h^2_{SNP} (SNP-based heritability) HF (heart failure) HUNT (Health Study Nord-Trøndelag) HERMES (Heart Failure Molecular Epidemiology for Therapeutic Targets) IVW (Inverse Variance Weighting) IL-1 (interleukin-1) LDSC (linkage disequilibrium score regression) LD (linkage disequilibrium) LDSC-SEG (LDSC applied to specifically expressed genes) LRT (likelihood ratio test) LAVA (Local Analysis of [co]Variant Annotation) LHC-MR (Latent Heritable Confounder Mendelian randomization) MAFLD (metabolic dysfunction-associated fatty liver disease) MR (Mendelian Randomization) MGI (Michigan Genome Initiative) MAF (minor allele frequency) MHC (major histocompatibility complex) MAGMA (Multi-marker Analysis of GenoMic Annotation) NAFLD (Non-alcoholic fatty liver disease) OR (odds ratios) PAD (peripheral artery disease) PLACO (Pleiotropic Analysis under a Composite Null Hypothesis) RDB (RegulomeDB) PP (posterior probabilities) *PNPLA3* (patatin-like phospholipase-domain containing protein 3) *PGC1* (PPARα/peroxisome proliferator-activated receptor-γ coactivator 1) ROS (reactive oxygen species) SNPs

(single nucleotide polymorphisms) *SAMM50* (sorting and assembly machinery component 50) SAM (Sorting and Assembly Machinery) TWAS (transcriptome-wide association study) ToppFun (ToppGene functional annotation tool) TFBS (transcription factor binding sites) T2D (Type 2 diabetes) TAG (triacylglycerol) TOM (translocator of the outer mitochondrial membrane) TG (triglyceride) UKB (UK Biobank) VTE (venous thromboembolism)

Acknowledgements

We would like to thank all GWAS authors who provided summary statistics for this study. We thank the Electronic Medical Records and Genomics (eMERGE) Network, the UK Biobank (UKB), the Estonian Biobank (EstBB), and the FinnGen Consortium for providing us with data on MAFLD, without whom this work would not have been possible. We would also like to thank the Health Study Nord-Trøndelag (HUNT), deCODE, Michigan Genome Initiative (MGI), DiscovEHR, UKB, and AFGen consortium for providing AF data; the CARDIoGRAMplusC4D and UKB consortium for providing CAD data; the deCODE for providing VTE data; the Heart Failure Molecular Epidemiology for Therapeutic Targets (HERMES) consortium for providing HF data; the Cardiovascular Disease Knowledge Portal (CVDKP) website for providing PAD data; and the GIGASTROKE consortium for providing stroke data.

References

[1] Eslam M, Newsome PN, Sarin SK, Anstee QM, Targher G, Romero-Gomez M, et al. A new definition for metabolic dysfunction-associated fatty liver disease: An international expert consensus statement. J Hepatol 2020; 73: 202-9.

[2] Eslam M, Sanyal AJ, George J. MAFLD: A Consensus-Driven Proposed Nomenclature for Metabolic Associated Fatty Liver Disease. Gastroenterology 2020; 158: 1999-2014.e1.

[3] Sanyal AJ, Castera L, Wong VW. Noninvasive Assessment of Liver Fibrosis in NAFLD. Clin Gastroenterol Hepatol 2023; 21: 2026-39.

[4] Ong JP, Pitts A, Younossi ZM. Increased overall mortality and liver-related mortality in non-alcoholic fatty liver disease. J Hepatol 2008; 49: 608-12.

[5] Deprince A, Haas JT, Staels B. Dysregulated lipid metabolism links NAFLD to cardiovascular disease. Mol Metab 2020; 42: 101092.

[6] Kasper P, Martin A, Lang S, Kütting F, Goeser T, Demir M, et al. NAFLD and cardiovascular diseases: a clinical review. Clin Res Cardiol 2021; 110: 921-37.

[7] Targher G, Byrne CD, Lonardo A, Zoppini G, Barbui C. Non-alcoholic fatty liver disease and risk of incident cardiovascular disease: A meta-analysis. J Hepatol 2016; 65: 589-600.

[8] Dongiovanni P, Petta S, Maglio C, Fracanzani AL, Pipitone R, Mozzi E, et al. Transmembrane 6 superfamily member 2 gene variant disentangles nonalcoholic steatohepatitis from cardiovascular disease. Hepatology 2015; 61: 506-14.

[9] Brouwers M, Simons N, Stehouwer CDA, Koek GH, Schaper NC, Isaacs A.

Relationship Between Nonalcoholic Fatty Liver Disease Susceptibility Genes and Coronary Artery Disease. Hepatol Commun 2019; 3: 587-96.

[10]Fang Z, Jia S, Mou X, Li Z, Hu T, Tu Y, et al. Shared genetic architecture and causal relationship between liver and heart disease. iScience 2024; 27: 109431.

[11]Hindley G, Frei O, Shadrin AA, Cheng W, O'Connell KS, Icick R, et al. Charting the Landscape of Genetic Overlap Between Mental Disorders and Related Traits Beyond Genetic Correlation. Am J Psychiatry 2022; 179: 833-43.

[12]Perry BI, Bowker N, Burgess S, Wareham NJ, Upthegrove R, Jones PB, et al. Evidence for Shared Genetic Aetiology Between Schizophrenia, Cardiometabolic, and Inflammation-Related Traits: Genetic Correlation and Colocalization Analyses. Schizophr Bull Open 2022; 3: sgac001.

[13]Hemani G, Bowden J, Davey Smith G. Evaluating the potential role of pleiotropy in Mendelian randomization studies. Hum Mol Genet 2018; 27: R195-r208.

[14]Ren Z, Simons P, Wesselius A, Stehouwer CDA, Brouwers M. Relationship between NAFLD and coronary artery disease: A Mendelian randomization study. Hepatology 2023; 77: 230-8.

[15]Peng H, Wang S, Wang M, Ye Y, Xue E, Chen X, et al. Nonalcoholic fatty liver disease and cardiovascular diseases: A Mendelian randomization study. Metabolism 2022; 133: 155220.

[16]Ghodsian N, Abner E, Emdin CA, Gobeil É, Taba N, Haas ME, et al. Electronic health record-based genome-wide meta-analysis provides insights on the genetic architecture of non-alcoholic fatty liver disease. Cell reports Medicine 2021; 2:

100437.

[17]Nielsen JB, Thorolfsdottir RB, Fritsche LG, Zhou W, Skov MW, Graham SE, et al. Biobank-driven genomic discovery yields new insight into atrial fibrillation biology. Nature genetics 2018; 50: 1234-9.

[18]Aragam KG, Jiang T, Goel A, Kanoni S, Wolford BN, Atri DS, et al. Discovery and systematic characterization of risk variants and genes for coronary artery disease in over a million participants. Nature genetics 2022; 54: 1803-15.

[19]Ghouse J, Tragante V, Ahlberg G, Rand SA, Jespersen JB, Leinøe EB, et al. Genome-wide meta-analysis identifies 93 risk loci and enables risk prediction equivalent to monogenic forms of venous thromboembolism. Nature genetics 2023; 55: 399-409.

[20]Shah S, Henry A, Roselli C, Lin H, Sveinbjörnsson G, Fatemifar G, et al. Genome-wide association and Mendelian randomisation analysis provide insights into the pathogenesis of heart failure. Nature communications 2020; 11: 163.

[21]van Zuydam NR, Stiby A, Abdalla M, Austin E, Dahlström EH, McLachlan S, et al. Genome-Wide Association Study of Peripheral Artery Disease. Circulation Genomic and precision medicine 2021; 14: e002862.

[22]Mishra A, Malik R, Hachiya T, Jürgenson T, Namba S, Posner DC, et al. Stroke genetics informs drug discovery and risk prediction across ancestries. Nature 2022; 611: 115-23.

[23]Auton A, Brooks LD, Durbin RM, Garrison EP, Kang HM, Korbel JO, et al. A global reference for human genetic variation. Nature 2015; 526: 68-74.

937 [24]Bulik-Sullivan BK, Loh PR, Finucane HK, Ripke S, Yang J, Patterson N, et al.
938 LD Score regression distinguishes confounding from polygenicity in genome-wide
939 association studies. Nature genetics 2015; 47: 291-5.
940 [25]Zhang Y, Qi G, Park JH, Chatterjee N. Estimation of complex effect-size
941 distributions using summary-level statistics from genome-wide association studies
942 across 32 complex traits. Nature genetics 2018; 50: 1318-26.
943 [26]Finucane HK, Reshef YA, Anttila V, Slowikowski K, Gusev A, Byrnes A, et al.
944 Heritability enrichment of specifically expressed genes identifies disease-relevant
945 tissues and cell types. Nature genetics 2018; 50: 621-9.
946 [27]Human genomics. The Genotype-Tissue Expression (GTEx) pilot analysis:
947 multitissue gene regulation in humans. Science (New York, NY) 2015; 348: 648-60.
948 [28]Chung D, Yang C, Li C, Gelernter J, Zhao H. GPA: a statistical approach to
949 prioritizing GWAS results by integrating pleiotropy and annotation. PLoS genetics
950 2014; 10: e1004787.
951 [29]Werme J, van der Sluis S, Posthuma D, de Leeuw CA. An integrated framework
952 for local genetic correlation analysis. Nature genetics 2022; 54: 274-82.
953 [30]Darrous L, Mounier N, Kutalik Z. Simultaneous estimation of bi-directional
954 causal effects and heritable confounding from GWAS summary statistics. Nature
955 communications 2021; 12: 7274.
956 [31]Ray D, Chatterjee N. A powerful method for pleiotropic analysis under composite
957 null hypothesis identifies novel shared loci between Type 2 Diabetes and Prostate
958 Cancer. PLoS genetics 2020; 16: e1009218.

959 [32]Watanabe K, Taskesen E, van Bochoven A, Posthuma D. Functional mapping and
960 annotation of genetic associations with FUMA. Nature communications 2017; 8:
961 1826.
962 [33]Kircher M, Witten DM, Jain P, O'Roak BJ, Cooper GM, Shendure J. A general
963 framework for estimating the relative pathogenicity of human genetic variants. Nature
964 genetics 2014; 46: 310-5.
965 [34]Boyle AP, Hong EL, Hariharan M, Cheng Y, Schaub MA, Kasowski M, et al.
966 Annotation of functional variation in personal genomes using RegulomeDB. Genome
967 research 2012; 22: 1790-7.
968 [35]Wang K, Li M, Hakonarson H. ANNOVAR: functional annotation of genetic
969 variants from high-throughput sequencing data. Nucleic acids research 2010; 38:
970 e164.
971 [36]de Leeuw CA, Mooij JM, Heskes T, Posthuma D. MAGMA: generalized gene-set
972 analysis of GWAS data. PLoS computational biology 2015; 11: e1004219.
973 [37]Gerring ZF, Mina-Vargas A, Gamazon ER, Derks EM. E-MAGMA: an
974 eQTL-informed method to identify risk genes using genome-wide association study
975 summary statistics. Bioinformatics (Oxford, England) 2021; 37: 2245-9.
976 [38]Schaid DJ, Chen W, Larson NB. From genome-wide associations to candidate
977 causal variants by statistical fine-mapping. Nature reviews Genetics 2018; 19:
978 491-504.
979 [39]Chen J, Bardes EE, Aronow BJ, Jegga AG. ToppGene Suite for gene list
980 enrichment analysis and candidate gene prioritization. Nucleic acids research 2009;

37: W305-11.

[40]Li Z, Shen W, Wu G, Qin C, Zhang Y, Wang Y, et al. The role of SAMM50 in non-alcoholic fatty liver disease: from genetics to mechanisms. FEBS Open Bio 2021; 11: 1893-906.

[41]Xu R, Kang L, Wei S, Yang C, Fu Y, Ding Z, et al. Samm50 Promotes Hypertrophy by Regulating Pink1-Dependent Mitophagy Signaling in Neonatal Cardiomyocytes. Front Cardiovasc Med 2021; 8: 748156.

[42]Patnaik D, Jena AB, Kerry RG, Duttaroy AK. In silico profiling of nonsynonymous SNPs of fat mass and obesity-associated gene: possible impacts on the treatment of non-alcoholic fatty liver disease. Lipids Health Dis 2023; 22: 17.

[43]Xu ZY, Jing X, Xiong XD. Emerging Role and Mechanism of the FTO Gene in Cardiovascular Diseases. Biomolecules 2023; 13.

[44]Bauer RC, Yenilmez BO, Rader DJ. Tribbles-1: a novel regulator of hepatic lipid metabolism in humans. Biochem Soc Trans 2015; 43: 1079-84.

[45]Zhang T, Tan P, Wang L, Jin N, Li Y, Zhang L, et al. RNALocate: a resource for RNA subcellular localizations. Nucleic acids research 2017; 45: D135-d8.

[46]Jiang J, Chen X, Li C, Du X, Zhou H. Polymorphisms of TRIB1 genes for coronary artery disease and stroke risk: A systematic review and meta-analysis. Gene 2023; 880: 147613.

[47]Krahmer N, Najafi B, Schueder F, Quagliarini F, Steger M, Seitz S, et al. Organellar Proteomics and Phospho-Proteomics Reveal Subcellular Reorganization in Diet-Induced Hepatic Steatosis. Dev Cell 2018; 47: 205-21.e7.

[48]Nguyen TB, Louie SM, Daniele JR, Tran Q, Dillin A, Zoncu R, et al. DGAT1-Dependent Lipid Droplet Biogenesis Protects Mitochondrial Function during Starvation-Induced Autophagy. Dev Cell 2017; 42: 9-21.e5.

[49]Alon L, Corica B, Raparelli V, Cangemi R, Basili S, Proietti M, et al. Risk of cardiovascular events in patients with non-alcoholic fatty liver disease: a systematic review and meta-analysis. Eur J Prev Cardiol 2022; 29: 938-46.

[50]Ciardullo S, Bianconi E, Cannistraci R, Parmeggiani P, Marone EM, Perseghin G. Peripheral artery disease and all-cause and cardiovascular mortality in patients with NAFLD. J Endocrinol Invest 2022; 45: 1547-53.

[51]Guo J, Ren W, Li A, Ding Y, Guo W, Su D, et al. Fat mass and obesity-associated gene enhances oxidative stress and lipogenesis in nonalcoholic fatty liver disease. Dig Dis Sci 2013; 58: 1004-9.

[52]Liu C, Mou S, Pan C. The FTO gene rs9939609 polymorphism predicts risk of cardiovascular disease: a systematic review and meta-analysis. PLoS One 2013; 8: e71901.

[53]Doney AS, Dannfald J, Kimber CH, Donnelly LA, Pearson E, Morris AD, et al. The FTO gene is associated with an atherogenic lipid profile and myocardial infarction in patients with type 2 diabetes: a Genetics of Diabetes Audit and Research Study in Tayside Scotland (Go-DARTS) study. Circ Cardiovasc Genet 2009; 2: 255-9.

[54]Witzel HR, Schwittai IMG, Hartmann N, Mueller S, Schattenberg JM, Gong XM, et al. PNPLA3(I148M) Inhibits Lipolysis by Perilipin-5-Dependent Competition with ATGL. Cells 2022; 12.

1025 [55]Huang Y, Cohen JC, Hobbs HH. Expression and characterization of a PNPLA3
1026 protein isoform (I148M) associated with nonalcoholic fatty liver disease. J Biol Chem
1027 2011; 286: 37085-93.
1028 [56]Simons N, Isaacs A, Koek GH, Kuč S, Schaper NC, Brouwers M. PNPLA3,
1029 TM6SF2, and MBOAT7 Genotypes and Coronary Artery Disease. Gastroenterology
1030 2017; 152: 912-3.
1031 [57]Kitamoto T, Kitamoto A, Yoneda M, Hyogo H, Ochi H, Nakamura T, et al.
1032 Genome-wide scan revealed that polymorphisms in the PNPLA3, SAMM50, and
1033 PARVB genes are associated with development and progression of nonalcoholic fatty
1034 liver disease in Japan. Hum Genet 2013; 132: 783-92.
1035 [58]Dai G, Liu P, Li X, Zhou X, He S. Association between PNPLA3 rs738409
1036 polymorphism and nonalcoholic fatty liver disease (NAFLD) susceptibility and
1037 severity: A meta-analysis. Medicine 2019; 98: e14324.
1038 [59]Krahmer N, Farese RV, Jr., Walther TC. Balancing the fat: lipid droplets and
1039 human disease. EMBO Mol Med 2013; 5: 973-83.
1040

Table 1. Genetic Correlation and Genetic Overlap Estimations Between 6 Pairwise Traits[a]

Trait pair	Genetic correlation				Genetic overlap		
	Genetic correlation (SE)	*P* value for LDSC	Intercept (SE)	*P* value for intercept	PM 11	PAR[b]	*P* value for GPA
MAFLD-AF	0.1381 (0.0891)	0.121	0.0080 (0.0053)	0.131	0.0000	0.0004	9.55×10^{-2}
MAFLD-CAD[c.d]	0.6266 (0.1375)	5.18×10^{-6}	0.0018 (0.0059)	0.760	0.0036	0.0424	7.12×10^{-31}
MAFLD-HF[c.d]	0.5725 (0.1576)	3.00×10^{-4}	0.0058 (0.0045)	0.197	0.0001	0.0010	1.12×10^{-11}
MAFLD-PAD[c.d]	0.6259 (0.2099)	2.90×10^{-3}	0.0075 (0.0053)	0.157	0.0001	0.0029	1.32×10^{-03}
MAFLD-Stroke[d]	0.2783 (0.1353)	3.98×10^{-2}	0.0057 (0.0045)	0.205	0.0001	0.0007	6.96×10^{-6}
MAFLD-VTE[c.d]	0.4844 (0.1220)	7.19×10^{-5}	0.0025 (0.0051)	0.624	0.0002	0.0025	4.66×10^{-10}

Note:

a. Genetic correlation and genetic overlap were estimated by LDSC and GPA methods, respectively. Bonferroni-corrected significance threshold was set at $P < 8.33\times10^{-3}$ (0.05/6), producing a final union set of 5 pairwise traits with significant genetic correlation or genetic overlap for subsequent analysis.

b. We introduced PAR as PM 11 / (PM 10 + PM 01 + PM 11) to represent the proportion of pleiotropic single-nucleotide variations (SNPs) associated with both traits against the proportion of SNPs associated with at least 1 trait.

c. Pairwise trait with significant genetic correlation.

d. Pairwise trait with significant genetic overlap.

Abbreviations: MAFLD, Metabolic dysfunction-Associated fatty liver disease; AF, Atrial fibrillation; CAD, Coronary artery disease; HF, Heart failure; PAD, Peripheral artery disease; VTE, Venous thromboembolism; LDSC, linkage disequilibrium score regression; GPA, genetic analysis incorporating pleiotropy and annotation method; PAR, pleiotropy association ratio; PM 11, proportion of genetic variants associated with both traits.

Figure legends

Figure 1. Metabolic dysfunction-associated fatty liver disease and six major cardiovascular diseases estimated by local genetic correlation.

LAVA volcano plots showing local genetic correlation coefficients (local-r_g*s*, y-axis) for MAFLD and CVDs with -log10 *p*-values for each trait pair of analyses for each locus. Loci above the horizontal line are significant at $P < 0.05$ (negative correlation for blue dots, positive correlation for red dots). Larger points with black circles indicate loci significantly associated after Bonferroni correction ($P = 6.49\times10^{-4} = 0.05 / 77$). LAVA-estimated local-rgs is shown on the blue-red scale. MAFLD, metabolic dysfunction-associated fatty liver disease; AF, atrial fibrillation; CAD, coronary artery disease; VTE, venous thromboembolism; HF, heart failure; PAD, peripheral arterial disease.

Figure 2. Inference of bidirectional causal relationship between metabolic dysfunction-associated fatty liver disease and six major cardiovascular diseases.

Forest plots of the causal relationship between MAFLD and six major CVDs using the LHC-MR method. The estimates presented in the forest plot were obtained using the LHC-MR method. A positive association is indicated by the odd ratio (OR > 1), while a negative association is indicated by OR < 1. The results of forward causality from the LHC-MR method are in the up panel, and the results of reverse causality from the LHC-MR method are in the down panel. MAFLD, metabolic dysfunction-associated fatty liver disease; AF, atrial fibrillation; CAD, coronary artery

disease; VTE, venous thromboembolism; HF, heart failure; PAD, peripheral arterial disease.

Figure 3. Manhattan plots for the PLACO results of metabolic dysfunction-associated fatty liver disease and six major cardiovascular diseases. Manhattan plots reflect chromosomal position (x-axis) and negative log10-transformed P-values (y-axis) for each SNP. The horizontal dashed red line indicates the genome-wide significant P-value of -log10 (5×10^{-8}). The r^2 threshold for defining independent significant SNPs was set to 0.2, and the maximum distance between LD blocks merged into one locus was set to 500 kb. The independent genome-wide significant associations with the smallest P-value (Top lead SNP) are encircled in a colorful circle. Only SNPs shared across all summary statistics were included. MAFLD, metabolic dysfunction-associated fatty liver disease; AF, atrial fibrillation; CAD, coronary artery disease; VTE, venous thromboembolism; HF, heart failure; PAD, peripheral arterial disease.

Figure 4. The overall situation of the pleiotropy association between metabolic dysfunction-associated fatty liver disease and six major cardiovascular diseases. A circular dendrogram showing the shared genes between MAFLD (center circle) and each of six CVDs (first circle), resulting in six pairs. A total of 49 shared loci were identified across six trait pairs (third circle), mapped to 45 nominally significant pleiotropic genes (34 were Bonferroni-corrected significant) identified by

multimarker analysis of GenoMic annotation (MAGMA). For the trait pairs with more than three pleiotropic genes, we only showed the top 3 pleiotropic genes according to the prioritization of candidate pleiotropic genes (fourth circle). MAFLD, metabolic dysfunction-associated fatty liver disease; AF, Atrial fibrillation; CAD, Coronary artery disease; VTE, Venous thromboembolism; HF, Heart failure; PAD, Peripheral artery disease.

Figure 1.

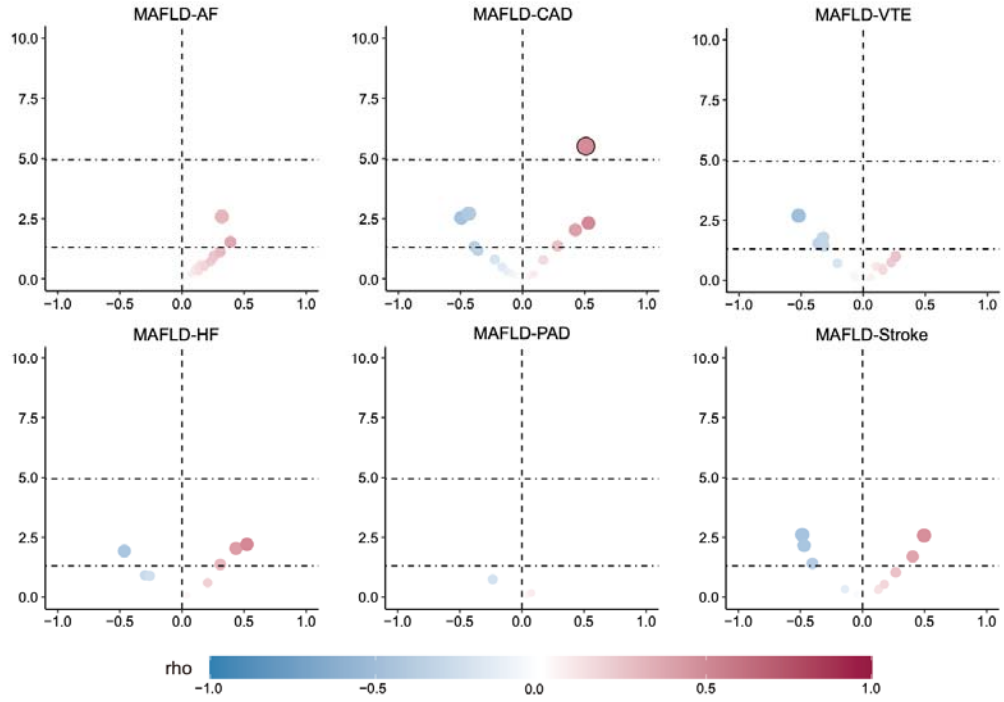

Figure 2.

Exposure	Outcome	OR (95% CI)	P value
NAFLD	AF	1.110 (1.043−1.177)	2.36e−03
NAFLD	CAD	1.368 (1.121−1.615)	1.31e−02
NAFLD	HF	1.003 (0.883−1.123)	9.67e−01
NAFLD	PAD	1.374 (1.211−1.537)	1.39e−04
NAFLD	VTE	1.307 (1.099−1.515)	1.13e−02
NAFLD	Stroke	1.281 (−0.246−2.808)	7.51e−01
AF	NAFLD	1.014 (0.969−1.059)	5.55e−01
CAD	NAFLD	1.102 (1.065−1.139)	6.30e−07
HF	NAFLD	1.128 (0.995−1.261)	7.61e−02
PAD	NAFLD	1.039 (0.965−1.113)	3.11e−01
VTE	NAFLD	1.107 (1.046−1.168)	9.94e−04
Stroke	NAFLD	1.076 (0.770−1.382)	6.39e−01

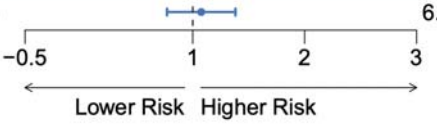

Figure 3.

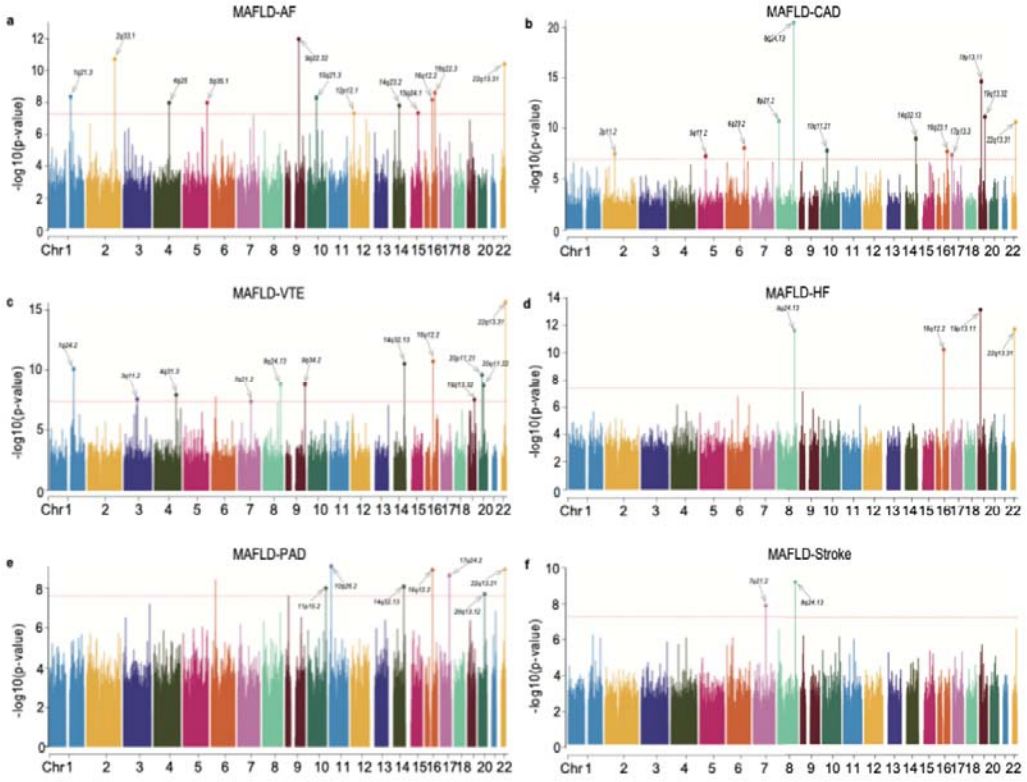

Figure 4.

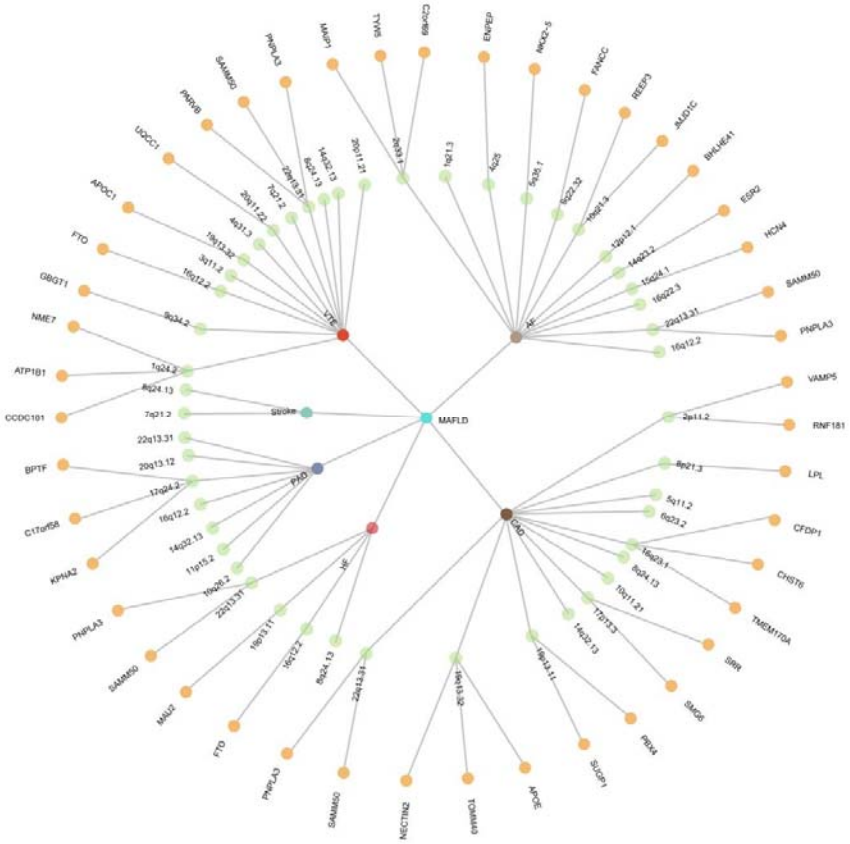

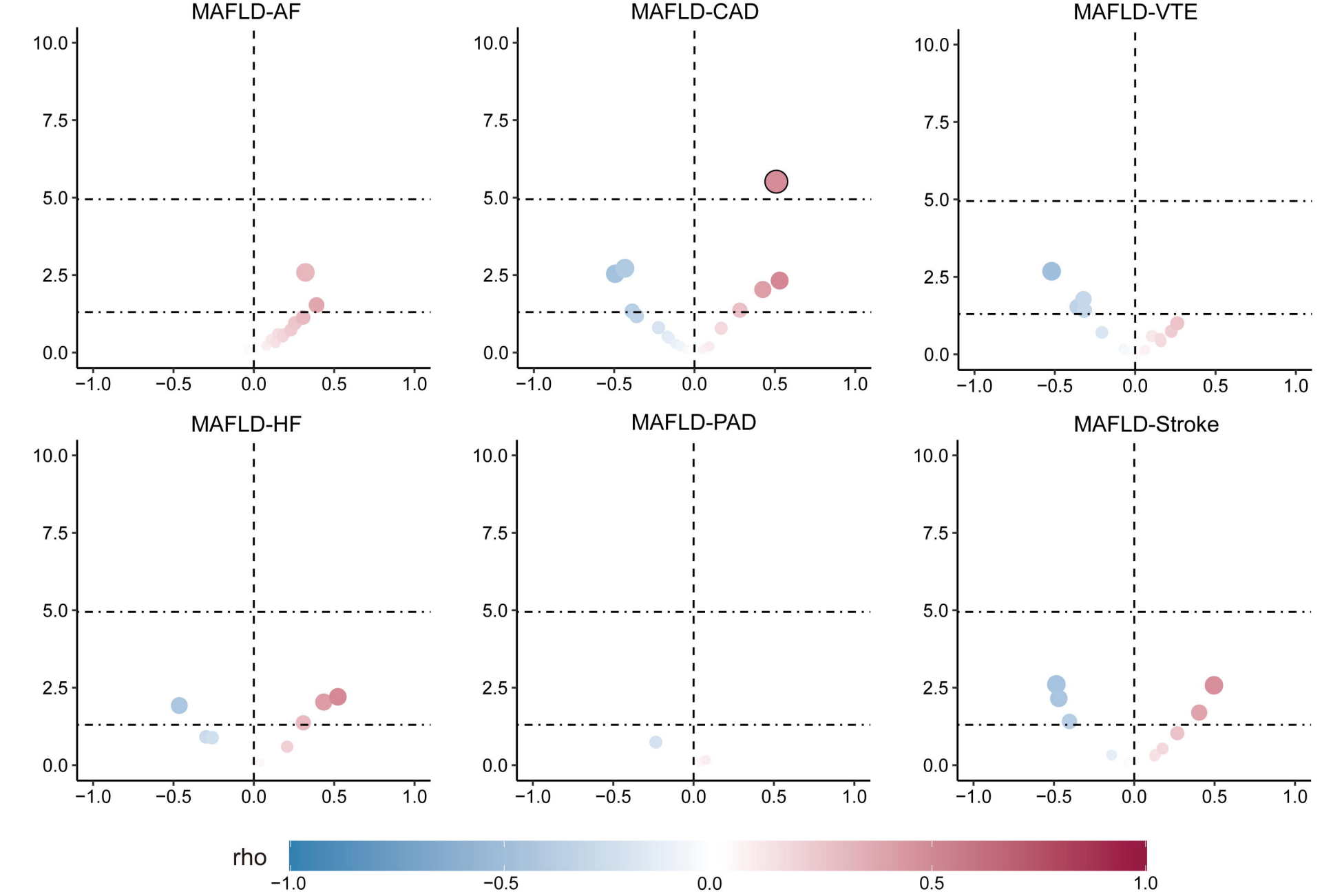
MAFLD-AF
MAFLD-CAD
MAFLD-VTE
MAFLD-HF
MAFLD-PAD
MAFLD-Stroke
10.0
7.5
5.0
2.5
0.0
−1.0
−0.5
0.0
0.5
1.0
rho

Exposure	Outcome	OR (95% CI)	P value
NAFLD	AF	1.110 (1.043−1.177)	2.36e−03
NAFLD	CAD	1.368 (1.121−1.615)	1.31e−02
NAFLD	HF	1.003 (0.883−1.123)	9.67e−01
NAFLD	PAD	1.374 (1.211−1.537)	1.39e−04
NAFLD	VTE	1.307 (1.099−1.515)	1.13e−02
NAFLD	Stroke	1.281 (−0.246−2.808)	7.51e−01
AF	NAFLD	1.014 (0.969−1.059)	5.55e−01
CAD	NAFLD	1.102 (1.065−1.139)	6.30e−07
HF	NAFLD	1.128 (0.995−1.261)	7.61e−02
PAD	NAFLD	1.039 (0.965−1.113)	3.11e−01
VTE	NAFLD	1.107 (1.046−1.168)	9.94e−04
Stroke	NAFLD	1.076 (0.770−1.382)	6.39e−01

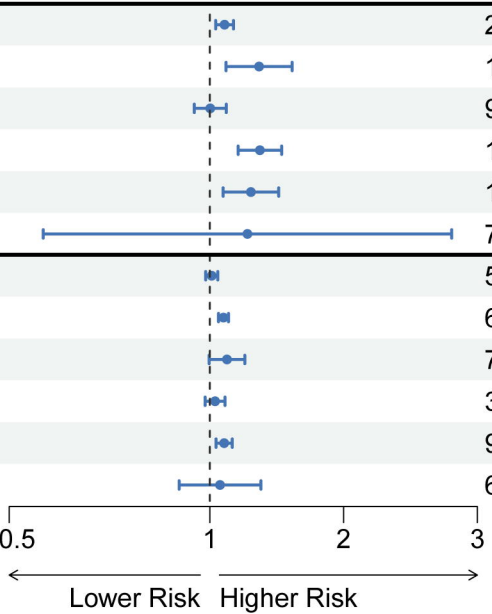

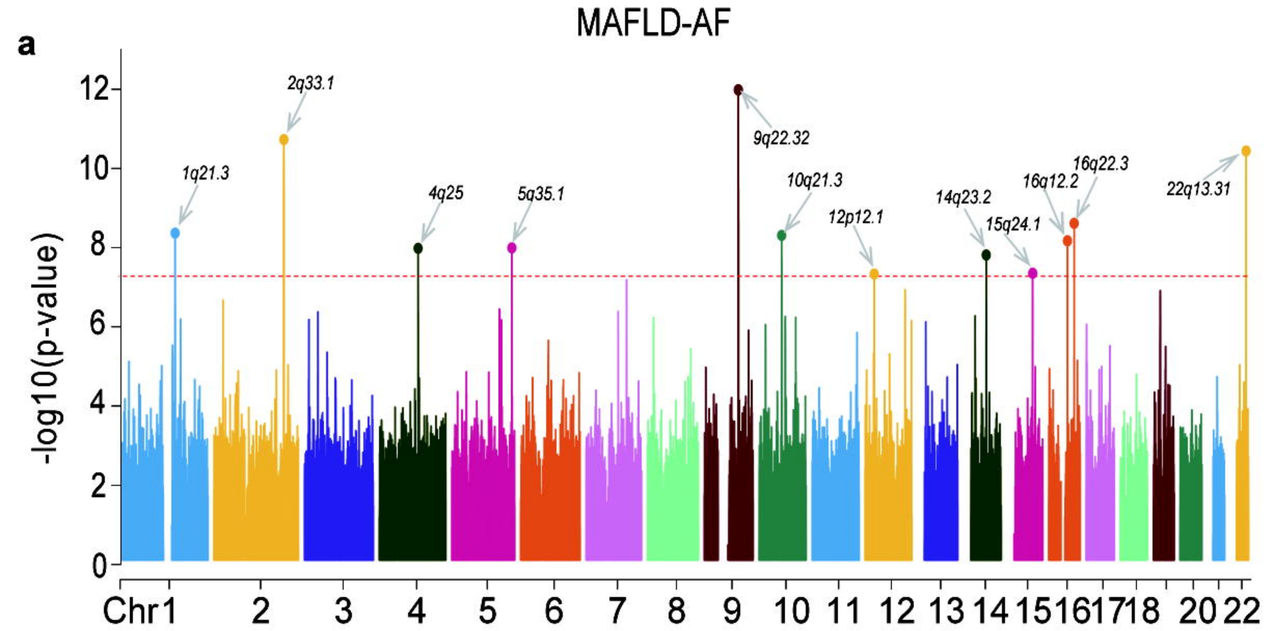

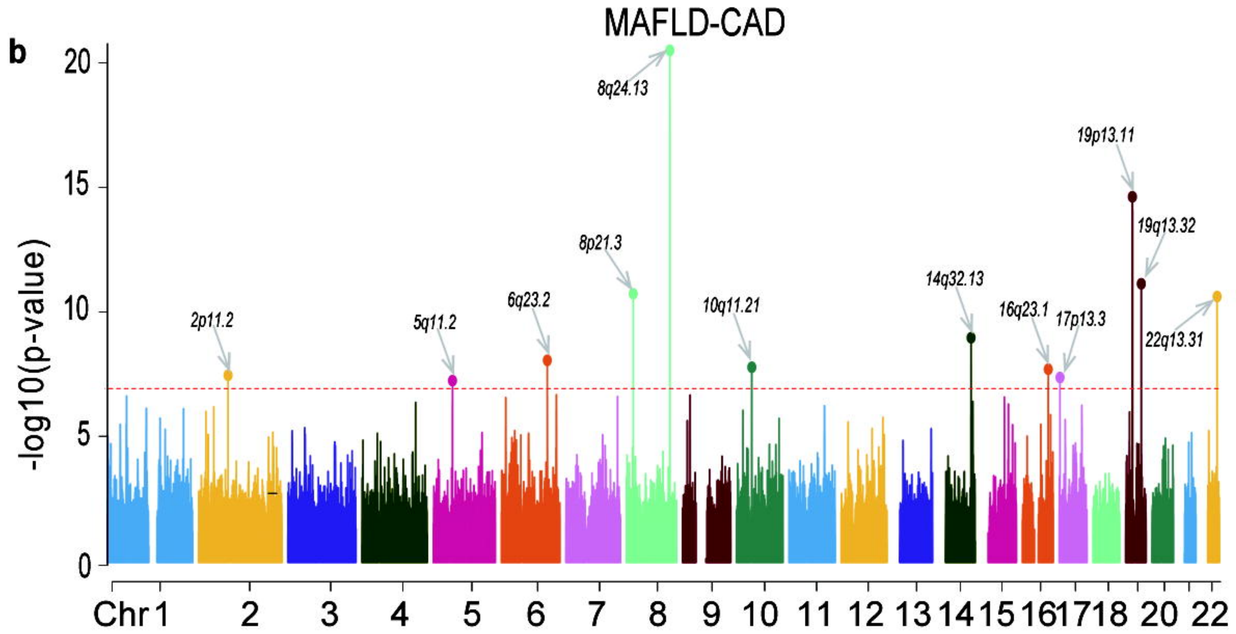

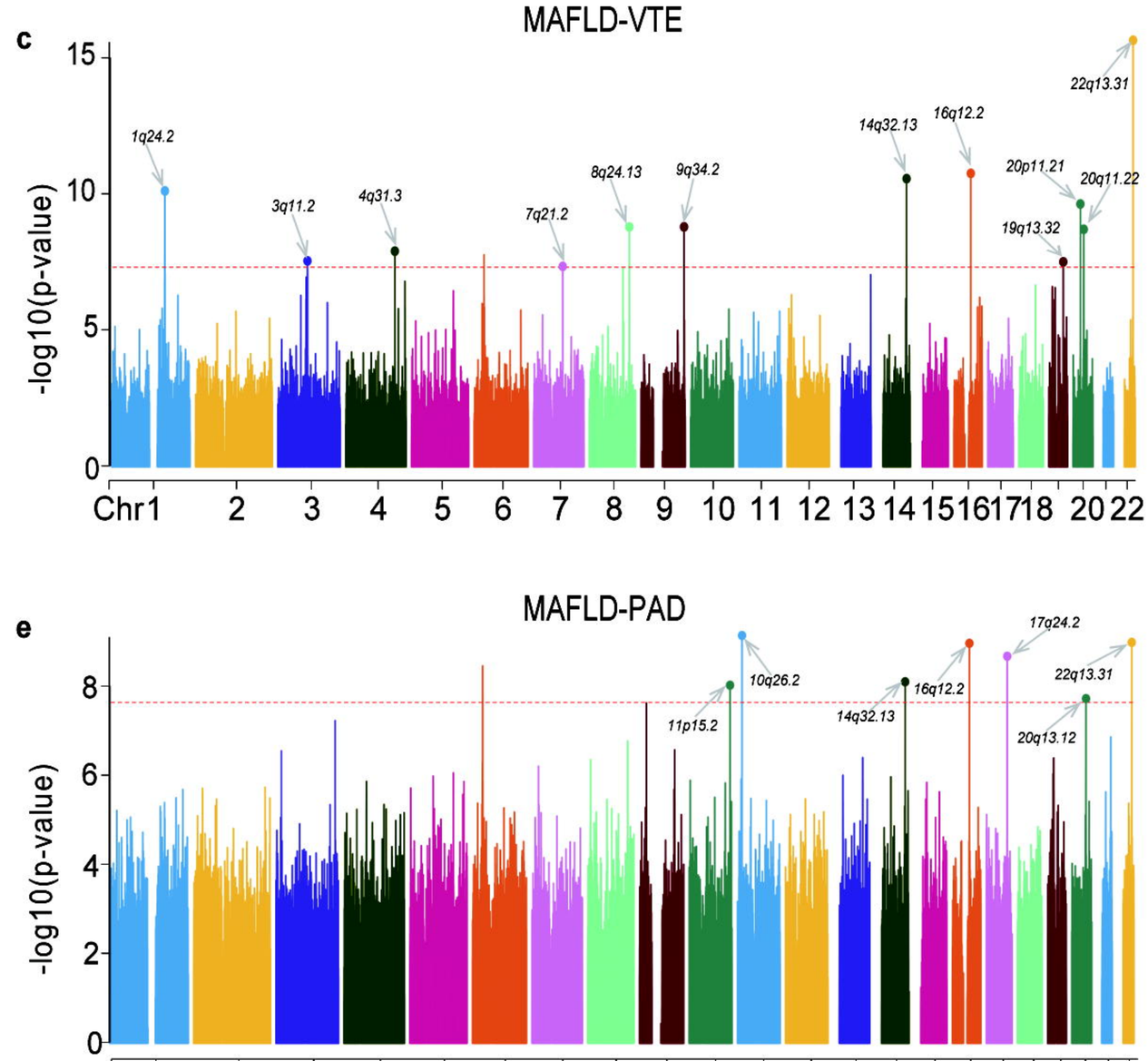

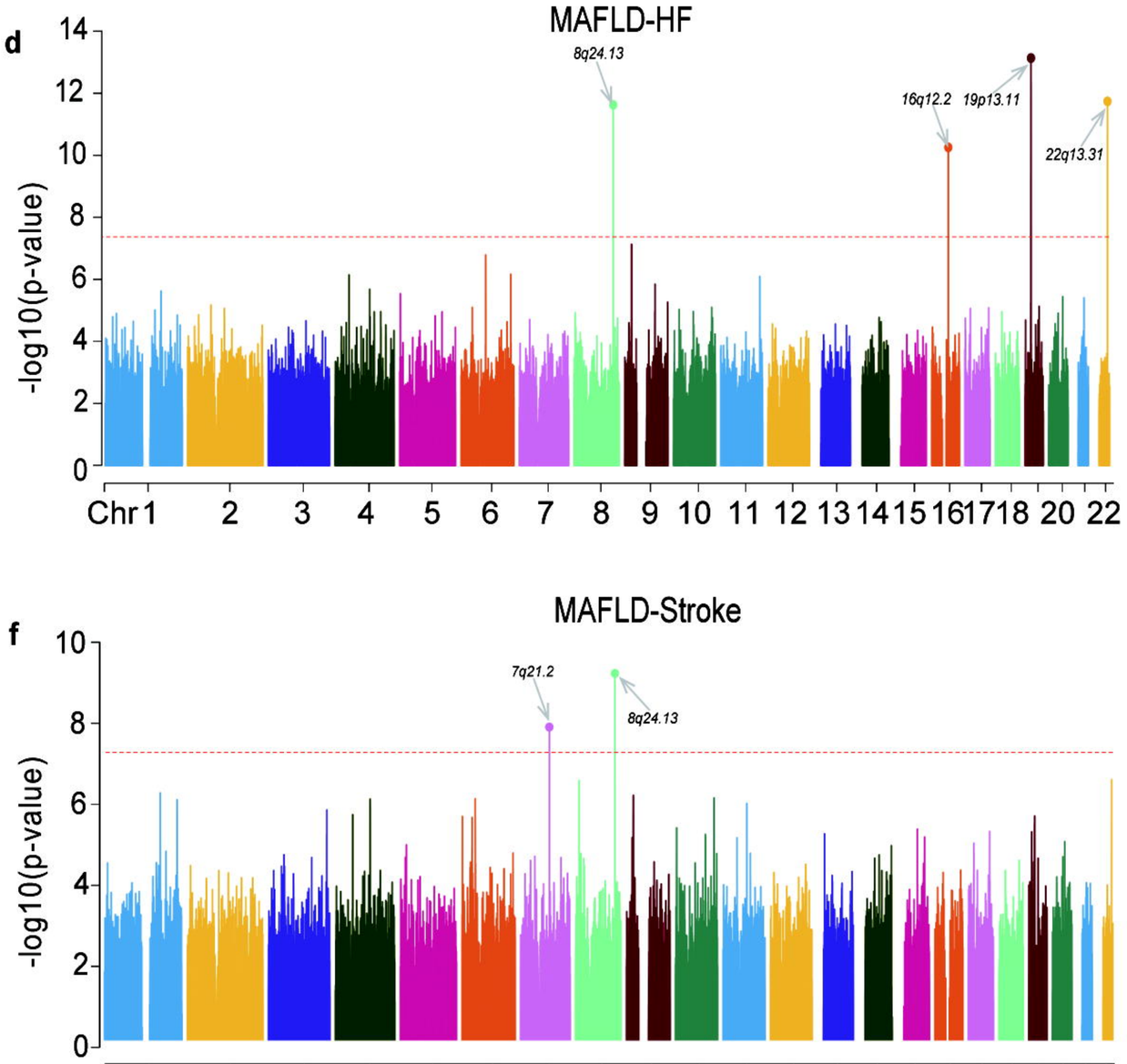


MAFLD
VTE
AF
Stroke
PAD
HF
CAD
MAIP1
TYW5
C2orf69
ENPEP
NKX2-5
FANCC
REEP3
JMJD1C
BHLHE41
ESR2
HCN4
SAMM50
PNPLA3
16q12.2
VAMP5
RNF181
LPL
CFDP1
CHST6
TMEM170A
SRR
SMG6
PBX4
SUGP1
APOE
TOMM40
NECTIN2
SAMM50
PNPLA3
FTO
MAU2
SAMM50
PNPLA3
KPNA2
C17orf58
BPTF
CCDC181
ATP1B1
NME7
GBGT1
FTO
APOC1
UQCC1
PARVB
SAMM50
PNPLA3
20p11.21
14q32.13
8q24.13
22q13.31
7q21.2
20q11.22
4q31.3
19q13.32
3q11.2
16q12.2
9q34.2
1q24.2
8q24.13
7q21.2
22q13.31
20q13.12
17q24.2
16q12.2
14q32.13
11p15.2
10q26.2
22q13.31
19p13.11
16q12.2
8q24.13
22q13.31
19q13.32
19p13.11
14q32.13
17p13.3
10q11.21
8q24.13
16q23.1
6q23.2
5q11.2
8p21.3
2p11.2
16q12.2
22q13.31
15q24.1
14q23.2
12p12.1
10q21.3
9q22.32
5q35.1
4q25
1q21.3
2q33.1

Metabolic dysfunction-associated fatty liver disease

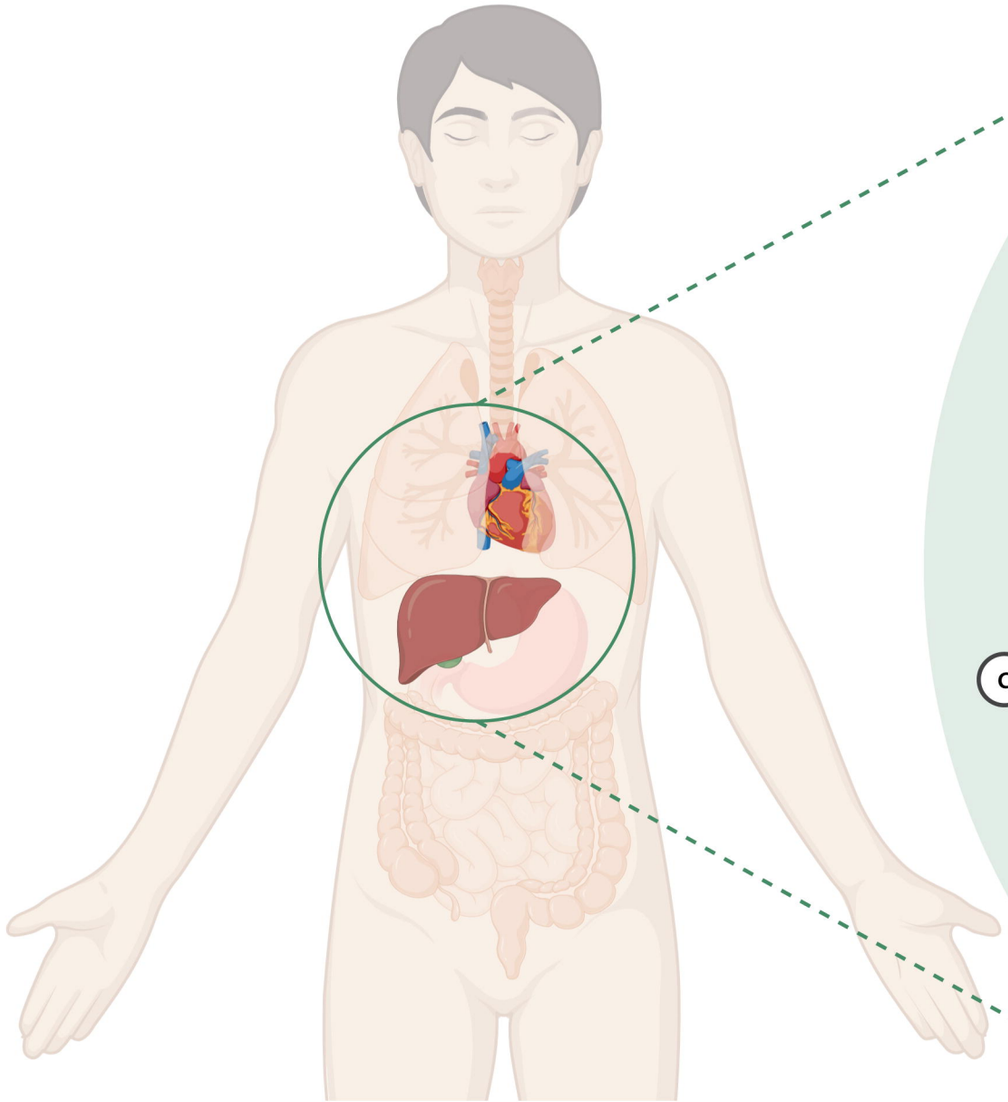

Cardiovascular diseases

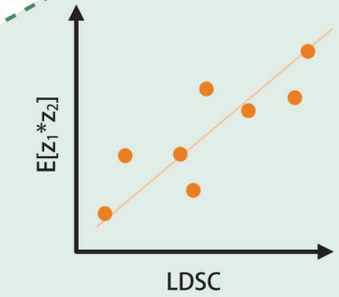

a Linkage disequilibrium score regression

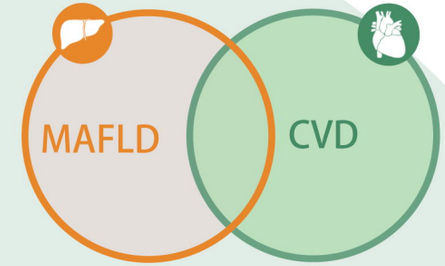

b Genetic analysis incorporating Pleiotropy and Annotation

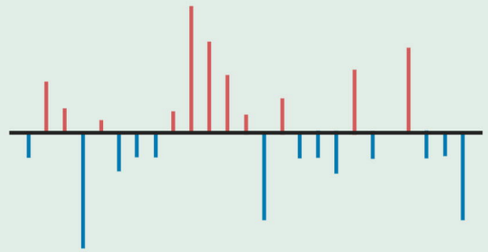

c Local Analysis of [co]Variant Annotation

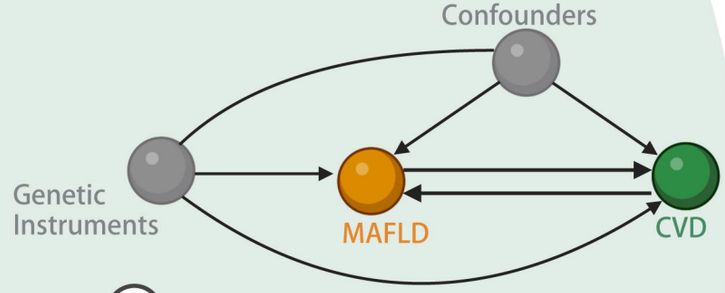

d Latent Heritable Confounder MR

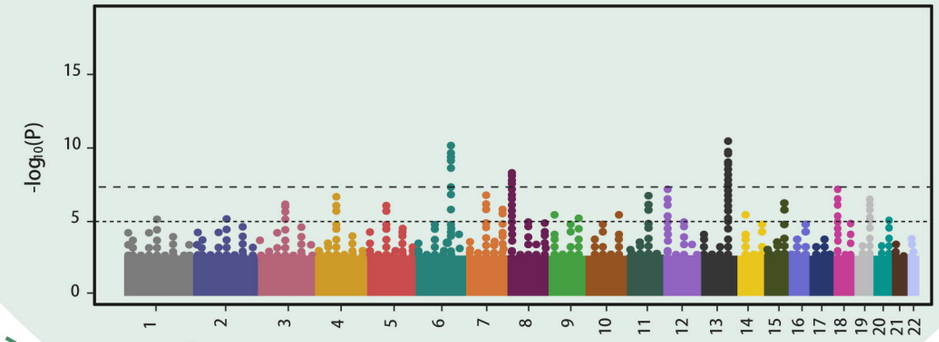

e Pleiotropic Analysis under a Composite Null Hypothesis